The University of Wisconsin
High-Power Microwave Transmission
And Mode Conversion Program

Progress Report

For the Period
January 1, 2013 – December 31, 2014

Department of Energy Contract DE-FG02-85ER52122

Ronald J. Vernon, Professor Emeritus

Principal Investigator

Phone: (608) 262-0774
Email: vernon@engr.wisc.edu

Department of Electrical and Computer Engineering
The University of Wisconsin
1415 Engineering Dr.
Madison, WI 53706

August 14, 2015

DOE/Office of Science Program Office: Research Division, SC-24.2
DOE/Office of Science Program Technical Program Manager Contact:
Barry Sullivan

Contributors to the Research Presented in this Report

Eric Buscarino

Dr. Bryan Fox
(Now working at MIT Lincoln Laboratory)

Dr. Shaolin Liao
(Now working at Argonne National Laboratory)

Dr. Michael Perkins
(Now working at Lawrence Livermore Laboratory)

Dr. Benjamin Rock
(Now working at the Naval Research Laboratory)

Dr. Ungku Fazri Ungku Farid

Professor Emeritus Ronald J. Vernon
(Principal Investigator)

Table of Contents

i. Project Objectives

The general objective of this project has been to develop improved designs, design tools and background theory for the microwave hardware and components associated with the DOE Plasma Fusion Program. We have developed the basic theory, software, fabrication techniques, and low-power measurement techniques for the design of microwave hardware associated with gyrotrons, microwave mode converters and high-power microwave transmission lines.

The significant progress that we have made in the development of improved launchers and mirror systems for TE_{0n} mode gyrotrons is also discussed and work will continue in this area. Such gyrotrons are in use at several facilities including HSX at the University of Wisconsin-Madison and new gyrotrons with these modes are being developed. We also report on our continuing investigation of traveling-wave resonators which would be valuable in testing components at high power (say 1-2 MW) with lower power gyrotrons (say 300 kW). This is general background work related to that proposed by Tim Bigelow at ORNL. Several other related tasks will also be discussed.

This has been a long term program. This report does not cover earlier work done on this project This work was covered in previous annual reports. Early publications are not listed here.

Even though Department of Energy funding for this long term project has ended, we believe that there are ways in which we can continue be a resource to the US gyrotron development program and ECRH transmission line community for various problems which may arise in the area of our expertise. Several problems which are of interest will be considered as time allows.

I. Introduction and Background

The report which follows gives a brief summary of some of the gyrotron related research which has been conducted at the University of Wisconsin mainly in 2013-2014 . Some of our earlier work, which is relevant to this recent research, is also presented. A brief listing of some of our plans for continued research is also presented. Reference will be made to the CPI gyrotron structure, which is shown schematically in Fig. 1 below. Our major concern in this report and proposal will be with the gyrotron section including the launcher and mirrors (usually four here), which together are sometimes called the quasi-optical mode converter. The numbering of the mirrors follows the beam path from the launcher with mirror M1 being closest to the launcher. This numbering will be used throughout the report.

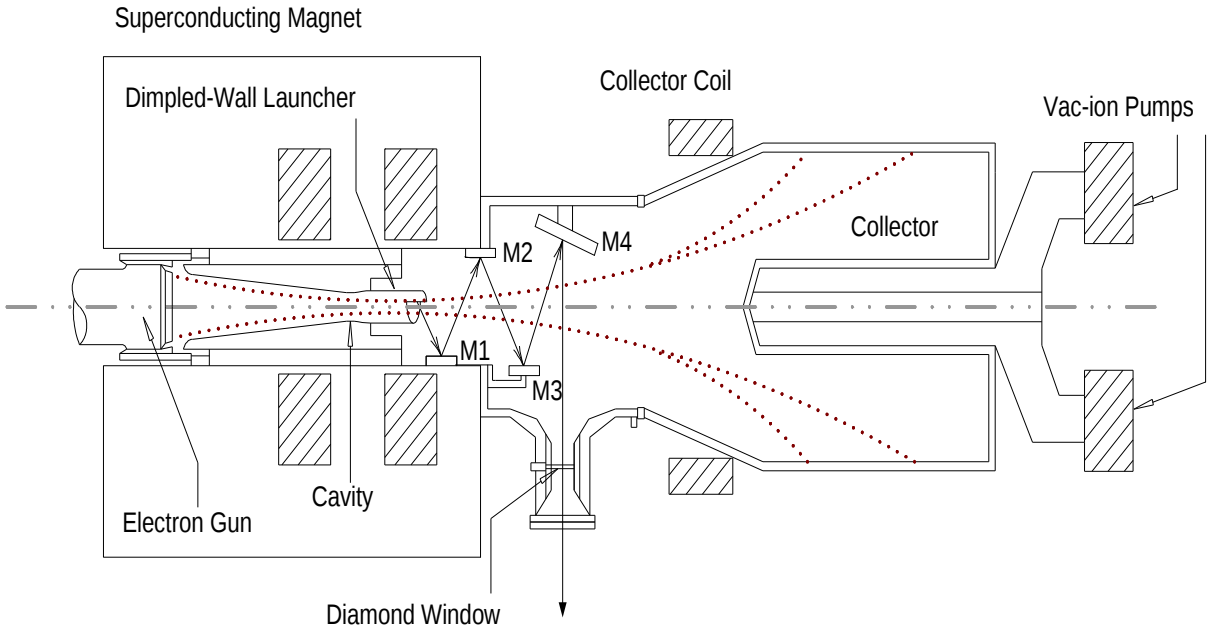

Fig. 1. Schematic drawing of a four-mirror CPI-type gyrotron. The arrows indicate the approximate microwave beam path out of the launcher, through the mirror system and out of the vacuum window.

Previously we developed an original design method for a sequence of three beam-shaping mirrors for possible use in the mode converter system of a gyrotron [1]. This type of mirror system with three beam shaping mirrors can yield improved performance over the use of a system with two beam shaping mirrors for some single mode/frequency beam transformations. Some beam transformations cannot be accomplished, even approximately, with only two shaping mirrors. For example, the transformation from a TEM_{22} to a TEM_{00} Gaussian mode cannot be achieved to even a rough approximation by a two-mirror beam shaping system. Because of such

limitations we have previously developed an algorithm for designing a three-mirror beam shaping system which is an extension to the two-mirror algorithm. We have found that a three-mirror beam shaping system can achieve the TEM_{22} to TEM_{00} transformation very well. In fact a three-mirror system could achieve most of the several transformations that we investigated to a good approximation. Also, a three-mirror system can often achieve a better output result than a two-mirror system even when the two-mirror system can obtain an adequate result. We will also discuss a mirror system design in this report that uses four beam shaping mirrors. (Note that although CPI gyrotrons often have four mirrors, only two of the mirrors are full beam shaping mirrors in most of their gyrotrons at this time.)

Also, in the past we have developed a technique for designing beam shaping mirror systems for cylinder-based mirrors. Previously all such beam-shaping mirror systems designs were for planar-based mirror systems. (By cylinder-based we mean that the mirrors are, to a first approximation, cylinders and the beam shaping capacity comes from small perturbations to this cylindrical surface. By planar-based we mean that the mirrors are, to a first approximation, planar and the beam shaping capacity comes from perturbations to this planar surface. In current four-mirror CPI gyrotrons, mirrors 1 and 2 are cylinder-based and mirrors 3 and 4 are planar-based.) Mike Perkins formerly of our group developed theory and codes to perform phase reconstruction from amplitude measurements of the launcher radiation made over several concentric cylinders. He also developed codes to design synthesized beam-shaping cylinder-based mirrors from this amplitude and phase distribution data. This gives us the capability to obtain synthesized beam shaping with mirrors 1 and 2 in CPI gyrotrons. The codes were applied to design a pair of cylinder-based mirrors compatible with use inside the bore of a CPI gyrotron. These bore mirrors were designed using the output of the launcher obtained with the Neilson Surf3d code. These mirrors have no discontinuities over their entire surface, a result obtained by the advanced phase unwrapping procedure developed by Mike Perkins. The experimental results were in good agreement with theoretical predictions. We have used these two capabilities to continue the development of multi-frequency beam-shaping reflector systems.

More recently we have developed a method of very rapidly simulating beam propagation from plane or cylindrical surfaces, which allowed us to consider even four shaping mirrors [2], [3]. This speed and added shaping surface becomes more useful when we consider mode converters for multi-frequency frequency gyrotrons, which is currently one of our major investigations. This work will be discussed further in the topics reported on below.

All of the above work has been reported in previous reports to the Department of Energy and in the articles listed in the Recent Publications Sections of this report.

II. Summary of Recent Gyrotron Related Research at The University of Wisconsin – Madison

A. Design of Quasi-Optical Mode Converters for Single and Multiple Frequencies (Ben Rock)

A-1. Introduction

In 2007 Ron Prater of General Atomics indicated the desirability of having a two frequency gyrotron on DIII-D. The 110 GHz frequency is the primary GA frequency and he suggested the second frequency should be about 125 GHz. (This frequency was later changed after work was well underway on our research on this subject.) Gyrotron cavity theory required the second gyrotron frequency be 124.5 GHz. Thus, the 110 and 124.5 GHz frequencies were used as a vehicle for the study and development of theory and computer programs for the design of quasi-optical mode converters for multi-frequency gyrotrons. Initially 127.5 GHz was also included since this was the frequency for the ITER start up gyrotrons. Later ITER abandoned the plan to use start-up gyrotrons. The initial design for our mode converter for the possible multi-frequency gyrotron was for frequencies of 107.5, 110, 124.5 and 127.5 GHz with the 110 and 124.5 GHz frequencies being emphasized. This work was done primarily by Shaolin Liao. New theory and computer programs were developed for this design [2]-[4] which allowed for rapid computation and having perturbations on all four mirrors. This had not been possible with previous methods.

An actual multi-frequency gyrotron which would be built by CPI would probably actually only operate at two frequencies. This is because a two-dielectric window with a fixed spacing can be used for two frequencies [29]. Such windows are simpler than other window types (variable gap and Brewster windows) which can accommodate more frequencies. Also two frequencies seem to be what is needed most at the moment by General Atomics. Ben Rock used the two-frequency case to improve on the design that Shaolin Liao developed earlier.

The operational frequencies and interaction modes of the gyrotron for this design are 110 GHz and 124.5 GHz in the $TE_{22,6}$ and $TE_{24,7}$ modes respectively. The optimization of the conversion system for this improved design was based on a new methodology in which the optimization of the launcher and mirror systems were integrated. By this it is meant that the optimization of these components was not separate, but rather, the optimization of each took into account the conversion properties of the other component. Another new feature of the new methodology is that the stray radiation within the gyrotron tube was explicitly minimized.

Stray radiation originates from spillover at the mirrors and truncation at the window aperture. If, as is typical, the output Gaussian is determined such that its −24 dB contour is at the window edge, roughly 0.4% truncation loss is foreordained when the conversion is perfect. When the conversion is imperfect, the true truncation loss can be somewhat more or less than this amount. A more tightly focused beam may place too much power density at the center of the window. Spillover losses originate because some power en route from the launcher misses the first mirror, and some power reflected from each mirror misses the next. In single frequency gyrotrons the diffractive (from spillover and truncation) losses can often be kept below 2% [1], [5], but in multi-frequency gyrotrons larger losses, 3% or more, are common [5]–[7]. For

operation at 1.5 MW output, 3% relative loss amounts to 45 kW of power which must then be dissipated within the gyrotron tube. Gyrotron designers are forced to include internal loads to absorb the power, which otherwise could cause overheating of the insulators and vacuum pumps, arcing, and discharges within the tube [6], [7]. It is also known that this power can disrupt the stable gyrotron operating regime and limit pulse time.

Despite the difficulties associated with stray radiation in the gyrotron tube, the conventional design procedure for internal mode conversion systems does not explicitly optimize to minimize losses. Rather, the typical optimization of the launcher is for Gaussian content in its radiated beam [5], [8], [9], while the conventional mirror synthesis procedures optimize for scalar coupling of the output beam to the Gaussian target distribution. The total losses in the converter are only checked after the design is complete and are then verified not to be excessive.

For multi-frequency conversion systems, the conventional optimization procedures are not necessarily commensurate with the goal of loss minimization and at some point a tradeoff typically occurs where the scalar coupling of the output beam is increased at the price of increased loss levels. There are two reasons for this. First, the results of Murphy [12] show that the best input to a mirror system, when a Gaussian output of the system is desired, is not necessarily also a Gaussian distribution. This implies that the traditional optimization of the launcher is suboptimal. Second, the scalar coupling is much more sensitive to phase distribution mismatch than to field amplitude distribution mismatch. In multi-frequency conversion systems it is common for the trajectories of the central rays at each frequency to be slightly skew. That is, at each frequency, the output beam has a slightly different exit angle. For the wide Gaussian targets typical for gyrotrons, this translates to relatively large phase mismatches, so optimizations based on the scalar coupling are likely to sacrifice field intensity (power) to achieve better phase distributions.

Our most recent work focuses on an alternate approach to converter design which we have used to improve the design of a dual-frequency mode conversion system. This approach introduces two new features to the design methodology. The first is that the launcher is not only optimized to produce Gaussian output, but rather it's optimization takes into account the conversion properties of the mirror system. The mirror system design intrinsically takes account of the conversion performed by the launcher so the new design methodology can be accurately described as an integrated approach. The other new feature of the integrated design approach is that the internal loss in the mirror system is explicitly minimized, and the power coupling to the desired target distribution is optimized afterward. This approach was capable of significantly reducing the diffractive losses in the design of the dual-frequency gyrotron, while maintaining over 99% Gaussian content in the output. The design process works by conducting a more thorough search of the parameter space of the converter. This is made possible by an ultra-fast implementation of the TIFFT algorithm for the evaluation of diffraction integrals [2], [3].

A-2. Converter System Optimization

The initial optimization of the launcher and mirror system was done following the conventional procedure. The launcher was first optimized with LOT [13] to produce an approximately Gaussian beam to feed the mirror system. The four mirrors were then optimized using a generalized Katsenelenbaum-Semenov (KS) algorithm [14] developed by our group

which converts the launched beam to an approximately Gaussian one at the gyrotron output window. In the conventional design procedure the optimization of the system is complete at this point, and in fact, the results of this step have previously been reported as a complete design by this group [1]. At this point, an additional optimization step was applied to both the launcher and mirrors. This was done by back-propagating the Gaussian targets through the mirror system obtained in the previous step. The routines of LOT were modified to optimize the launcher using the power coupling with these back-propagated fields as the objective. The new launcher output was subsequently used to further optimize the mirror system. The second mirror optimization proceeded in two steps. First, the mirrors were modeled as splines and a quasi-Newton algorithm was used to optimize the spline coefficients so that the mirrors guided maximum power through the window aperture. The output beams after this step were used to define Gaussian targets for a final optimization using the KS algorithm. After this process, the converter design is complete. The ability to synthesize all four mirrors using the Quasi-Newton algorithm requires the ability to propagate the launched beam through the mirror system very quickly. The ultra-fast implementation of the TIFFT algorithm [2], [3] was written to allow this method to be feasible.

A-3. Dual-Frequency Design Results

The original mode conversion system designed by Liao, Vernon and Neilson [3] was among the best (by some measures the best at the time of its completion), but as indicated in Table I it suffers from a fairly large amount of loss, particularly at 110 GHz. The integrated design algorithm was employed to re-optimize this system minimizing power loss. The resulting conversion properties are shown alongside those for the previous design in Table I. The integrated design reduced the loss by 1.1% at 110 GHz and 0.4% at 124.5 GHz. The Gaussian content was actually increased slightly, but meaningfully at 110 GHz, while remaining essentially unchanged at 124.5 GHz.

TABLE I
SUMMARY OF THE RESULTS OF THE INTEGRATED CONVERSION SYSTEM DESIGN COMPARED WITH THOSE FOR THE PREVIOUS DESIGN. THE GAUSSIAN CONTENT IS THE VECTOR COUPLING OF THE SYSTEM OUTPUT WITH A SHIFTED AND TILTED GAUSSIAN WITH ITS 2.63 CM WAIST RADII AT THE WINDOW

	Previous Design		Integrated Design	
Frequency (GHz)	110	124.5	110	124.5
Spillover loss at M1 (%)	1.17	0.55	1.10	0.55
Spillover loss at M2 (%)	0.42	0.40	0.17	0.20
Spillover loss at M3 (%)	1.01	0.64	0.57	0.43
Spillover loss at M4 (%)	0.21	0.18	0.13	0.11
Truncation loss at window (%)	1.01	0.65	0.71	0.71
Cumulative loss	3.76	2.41	2.68	1.98
Gaussian Content (%)	99.19	99.32	99.62	99.28
Conversion Efficiency (%)	95.46	96.92	96.95	97.31
α_z (°)	0.16	0.15	0.04	− 0.03
α_x (°)	0.41	−0.44	0.38	− 0.47
δ_z (mm)	1.89	0.48	0.31	− 0.83
δ_x (mm)	1.66	− 0.30	0.93	− 0.20

There are azimuthal angular tilts and spatial shifts for each beam in both systems. These angles and shifts originate from the slightly different Brillouin properties of the waveguide modes. The azimuthal tilts (α_x) are roughly the same for both converter designs, and the azimuthal shifts (δ_x) were slightly decreased by the integrated design. The longitudinal tilts (α_z) were reduced for the integrated design, but they could also have been removed from the original system by applying a slight rotation to the fourth mirror of that system. The final converted fields at the window are shown in Figs. 2 and 3 for both frequencies. This work was presented at the IRMMW Conference in Oct. 2011 in Houston [15] and in a paper accepted for publication in the IEEE Trans. on Plasma Science [16].

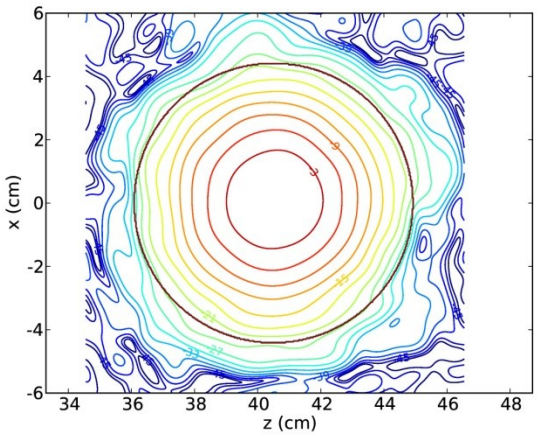

(a) 110 GHz

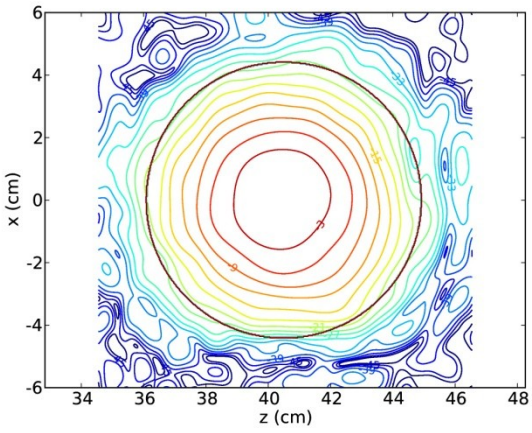

(b) 124.5 GHz

Fig. 2. The simulated dominant E_x component of the fields at the output of the conversion system at the window plane for both frequencies. The heavy circle indicates the extent of the window aperture. The contours are in 3 dB increments from -3 to -48 dB.

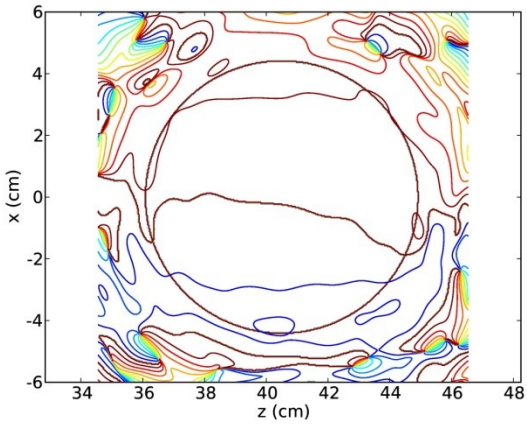

(a) 110 GHz

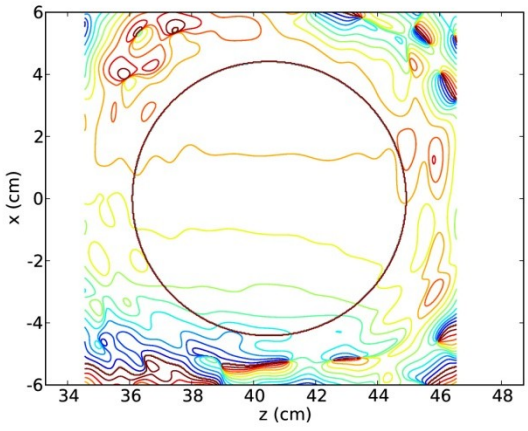

(b) 124.5 GHz

Fig. 3. The simulated phase distributions of the converter output fields (E_x) at the window plane for both frequencies. The contours are in 30° increments.

A-4. Low-Power Measurement Results (Bryan Fox)

At the time the integrated launcher and mirror system design was completed, our program did not have sufficient funding to have the launcher fabricated. The MIT Gyrotron Group (headed by Richard Temkin) wanted to use the new converter design in a two-frequency gyrotron experiment performed on a high-power short-pulse gyrotron at MIT. They agreed to have the launcher and mirror system fabricated for use in their gyrotron. There was a delay in the fabrication and the launcher was just finished in October 2012. It was sent to UW for cold testing. By this time Ben Rock had received his PhD and left our group for work at the Naval Research Lab in Washington. Bryan Fox made the measurements on the new launcher. Some of the results are shown below. For best agreement, the simulated date was shifted by 1 degree and 1.5 mm in z. This is approximately within our range of measurement error. The inner contours are quite close and the outer two or three contours represent such low power densities the neither the measurement of simulation results are accurate. The 1.5 mm and 1º differences may be due to measurement error, simulation error or fabrication error or some of all three. It is not possible to tell what the mix is. However the results were good enough to continue with the plan to use the launcher in the MIT gyrotron.

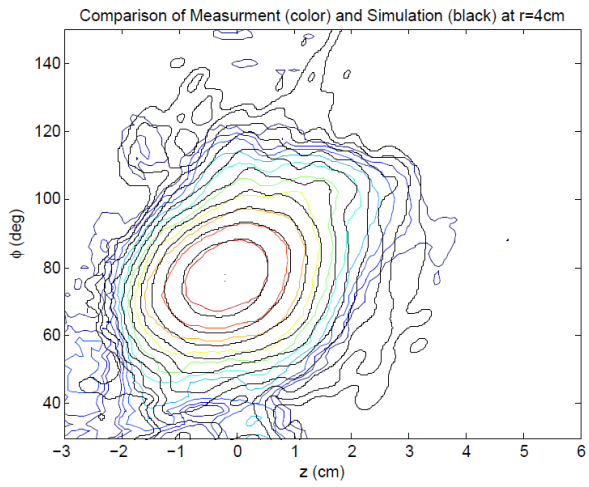

Fig. 4. Comparison of the measured (colored contours) and simulated (black contours) output contour plots for the two-frequency integrated design launcher at 110 GHz on a cylinder of 4 cm radius. The contours are in 3 dB increments from
-3 dB (inner) down to -30 dB.

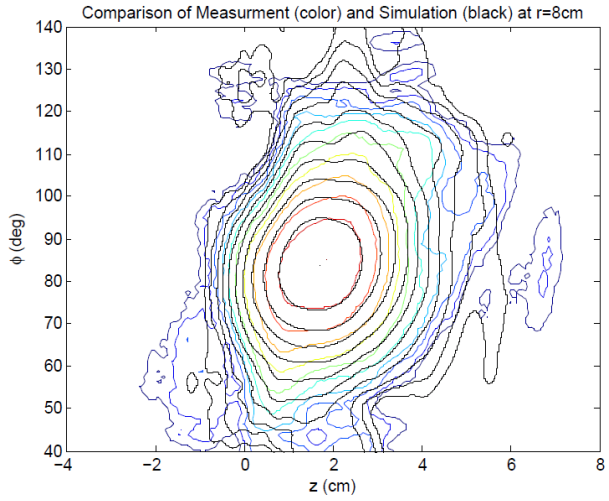

Fig. 5. Comparison of the measured (colored contours) and simulated (black contours) output contour plots for the two-frequency integrated design launcher at 110 GHz on a cylinder of 8 cm radius. The contours are in 3 dB increments from
-3 dB (inner) down to -30 dB.

A-5. Measurements at Pulsed High Power

After the measurements discussed in Sec. A-4 were made at UW, the mirror assemblies were sent to MIT for the high-power pulsed measurements inside their MW pulsed gyrotron. The results of these measurements were excellent at 110 GHz and reasonably good at 124.5 GHz. The results of these measurements were published in a paper in the IEEE Transactions on Plasma Science in May 2014 ref X.

Table II. Simulated and Measured Results for the Dual-Frequency Converter

	Simulation-UW	Cold Test-MIT	Hot Test - MIT
110 GHz			
Gaussian Coupling	**99.6 %**	**99 %**	**97.7%**
Offset Δx / Δz (mm)	**0.86 / 0.22**		**-1.7 / -2.5**
Tilt θ_x / θ_z (deg)	**0.38 / 0.04**	**0.3 / 0.6**	**0.08 / 0.01**
124.5 GHz			
Gaussian Coupling	**99.3 %**		**97%**
Offset Δx / Δz (mm)	**0.28 / 0.67**		**-9.0 / -2.5**

B. A

New Method for the Analysis of Perturbed-Wall Waveguide Mode Converters (Ben Rock)

An improved method for the analysis of the fields within a section of nonuniform cylindrical waveguide was developed. The technique uses the method of successive approximations to obtain consistent solutions to the Stratton–Chu equations and the cylindrical harmonic representations of the fields that satisfy Maxwell equations and the boundary conditions of the nonuniform waveguide. As opposed to some recently reported methods, [18], [21], this new method is not restricted to oversized waveguide structures and can directly evaluate the fields within a tapered section of waveguide. The method is validated by evaluating the fields within two different mode converters for gyrotron launchers. The accuracy is found to be competitive with the commercial method of moments code, Surf3d, but is faster and requires only a fraction of the computational resources. The development is very mathematical and not suitable for presentation in this report. Fig. 6 below is a comparison of the results from the new method and Surf3d for a $TE_{22,6}$ launcher at 110 GHz. The scalar coupling between these fields is 99.9%. Preliminary results of this work were presented in [23] and the work is presented in detail in [24].

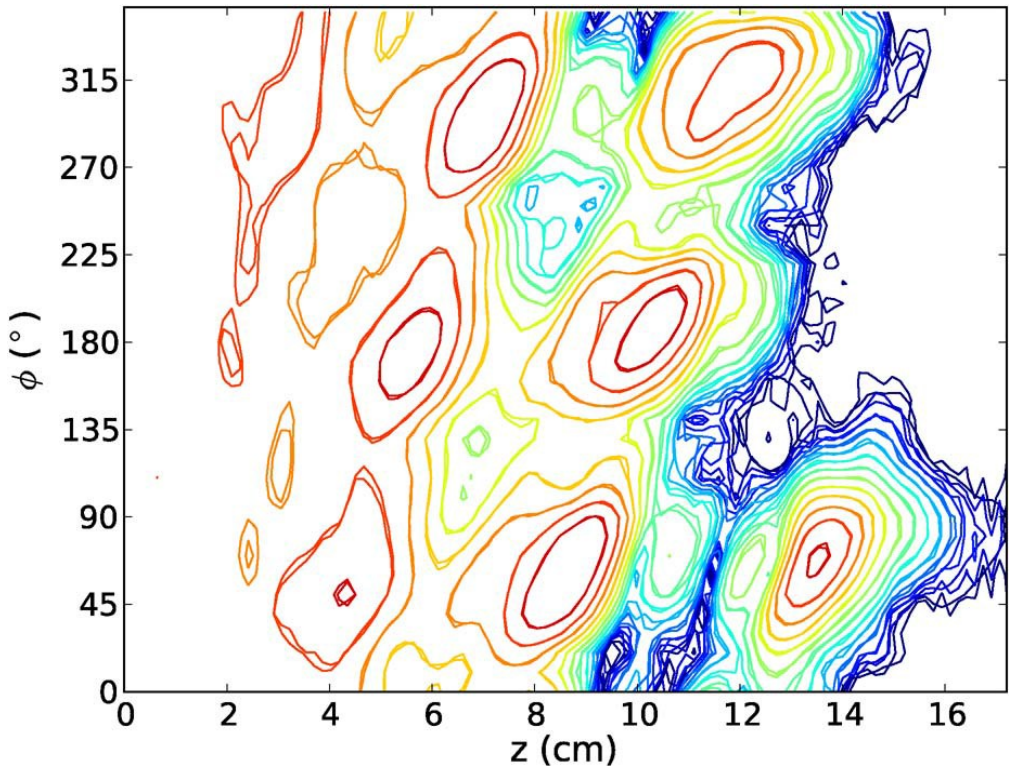

Fig. 6. H_z fields within a $TE_{22,6}$ launcher at $\rho = 0.85a_0$. Field distributions evaluated by the iterative Stratton–Chu method and by Surf3d are shown. The scalar coupling between these fields is 99.9%. The contours are in −3-dB increments from −3 to −39.

C. Launcher Design for TE_{0n} Mode Gyrotrons (Ungku Fazri Ungku Farid)

Unlike high-order rotating-mode spiral-cut launchers (e.g. for the $TE_{22,6}$ mode), not much work has been done for TE_{0n} mode launchers. (These launchers usually have a step-cut profile as there base geometry as shown in Fig. 7.) However, TE_{0n} mode gyrotrons are still used in several facilities such as HSX at the University of Wisconsin-Madison and lower power TE_{0n} mode gyrotrons are still being designed. In this research we have developed a new improved algorithm (based on work of Jin et. al [10], Rock and Vernon [24], and Denisov et. al. [20]) to design waveguide wall perturbations for launchers with this type of mode. A test design for a TE_{02} launcher with a radius of 1.3895 cm at 60 GHz for an improved Gaussian beam output pattern has been developed. This algorithm is loosely based on the generalized phase-correcting Katsenelenbaum-Semenov (K-S) mirror design algorithm [14]. This is a case where the mode is well above cutoff making the problem more difficult and the methods of Jin and Denisov do not work well. However, this is the situation that exists when conversion to a Gaussian beam must take place outside the gyrotron and may exist inside a gyrotron as well.

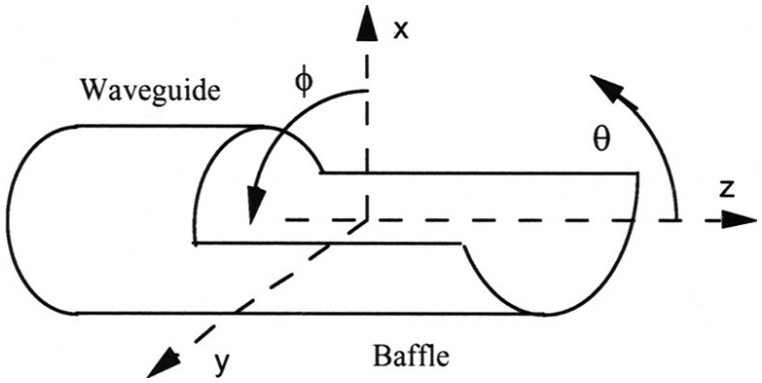

Fig. 7. Drawing of a simple step-cut TE_{02}-type Vlasov launcher with coordinate system used.

For a simple unperturbed TE_{02} launcher, the output radiation field is double-peaked (far from being Gaussian), spread out azimuthally more than 180^o and has many substantial side lobes (see Figs. 8 and 9). These factors pose a problem for the reflector that immediately follows the launcher because much of the power does not strike the reflector and is therefore lost. Furthermore, the many side lobes cannot be converted into a good Gaussian beam by a simple system of mirrors. We have developed a method of designing perturbations that results in a launcher output with an azimuthally narrower Gaussian-like beam with fewer and lower side lobes that can be more fully captured and more readily shaped by a mirror system.

A modified version of the K-S algorithm combined with a fast (FFT based) field propagation algorithm was applied to design the perturbations. Each Brillouin zone in the launcher (See Sec. E for further discussion of Brillouin zones.) is treated as a distinct mirror surface with the perturbations acting as simple phase shifters. An ideal Gaussian target beam is back-injected into the output aperture, and in each propagation step, the phase difference between the output target and propagated fields on the relevant Brillouin zone is transformed into perturbations. However, this method coupled with the far from cut-off nature of this launcher (f_c = 24.1 GHz, f = 60 GHz) results in impractically large and discontinuous perturbations. To overcome these problems, the maximum amplitude of the perturbations is capped and an elliptical Gaussian low-pass spatial filter is utilized at the last step to remove any spatial discontinuities or rapid perturbations. Filtering and controlling the amplitude of the perturbations degrades the Gaussian content of the output beam, but is necessary for a practical device. Finally all radiation patterns are independently verified with a widely-used Method-of-Moments based simulation software called Surf3d. Preliminary results of this research were presented at the IRMMW Conference in Houston in Oct. 20, 2011 [25] and later results were presented at the IRMMW Conference of Sept. 2012 [26]. A summary of the work was also presented at the US Gyrotron Community Meeting in Oak Ridge TN, May 2014.

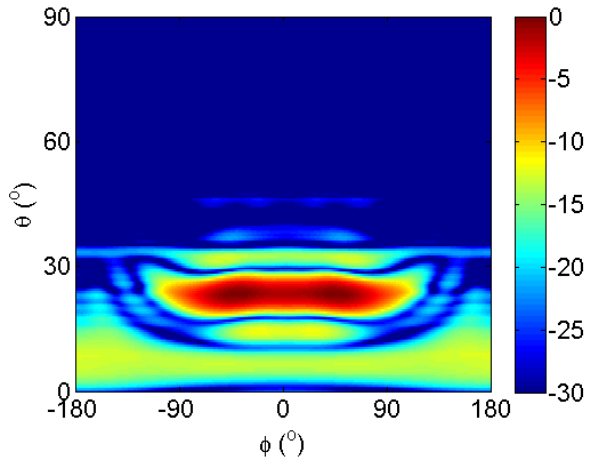

Fig. 8. The far-field pattern of $|E_\varphi|$ (co-polarization) of the smooth-wall 60 GHz, TE_{02} launcher (in dB) from Surf3d. Note the unacceptably wide main lobe and the number of significant side lobes.

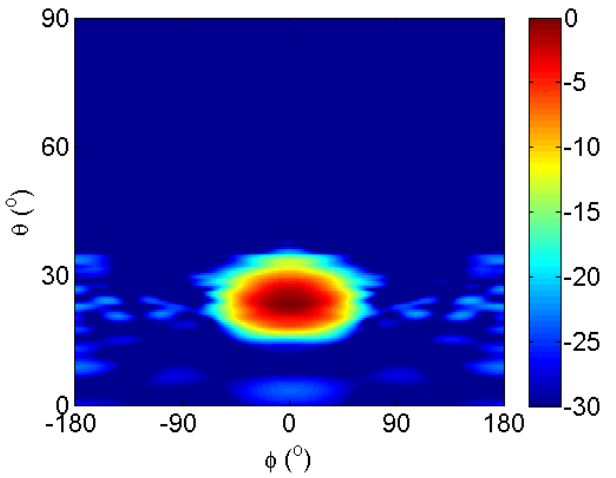

Fig. 9. The far-field pattern of $|E_\varphi|$ (co-polarization) of the perturbed-wall 60 GHz, TE_{02} launcher (in dB) from Surf3d. Note the narrower main lobe and the absence of significant side lobes.

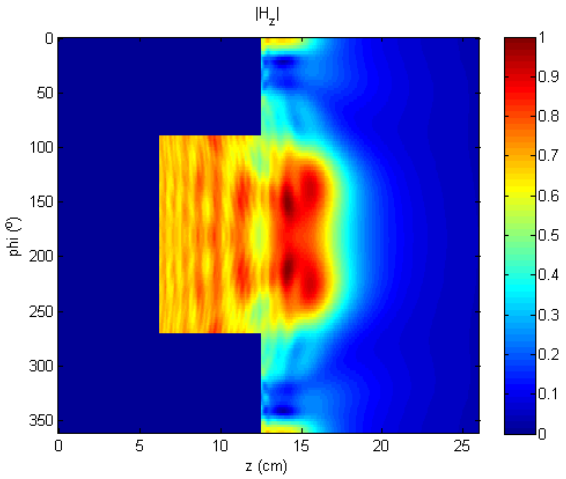

Fig. 10. The $|H_z|$ fields for a smooth-wall 60 GHz, TE_{02} launcher at the output aperture obtained using Surf3d (for a linear amplitude scale).

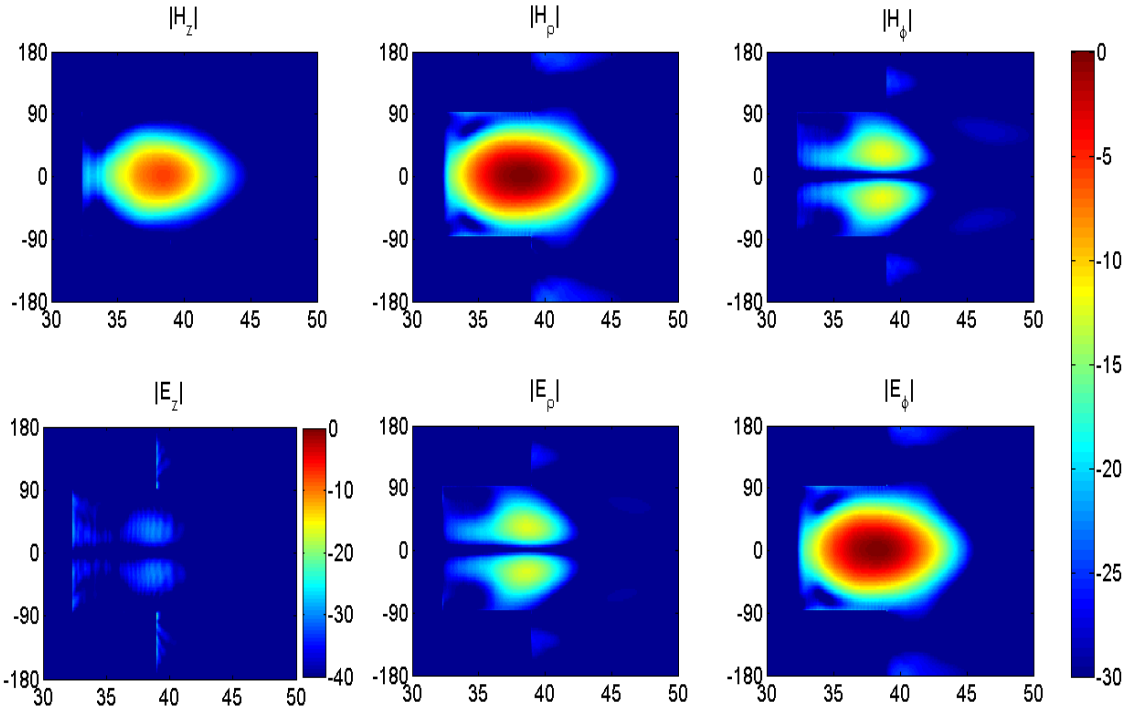

Fig. 11. All six field components at the launcher output aperture (in dB) from Surf3d. (Fields on the launcher walls are blanked out because Surf3d does not give accurate values there). The vertical axes are φ (°) and the horizontal-axes are z (cm). The scale of $|E_z|$ is expanded to -40 dB because $|E_z|$ is small.

Table III. Summary of the Far-field Comparison between the HSX Launchers.

Launcher	Co-polarization (E_φ)					Cross-polarization (E_θ)	
	Main Lobe Power	Directivity (dBi)	10 dB Angular Spread		Polar Exit Angle	$\lvert E_\theta \rvert$ max	Total Power
			Δφ	Δθ			
Smooth-Wall	79.38%	21.5	208.4°	8.5°	23.5°	-20.0 dB	0.09%
Perturbed	99.67%	23.5	91.2°	14.3°	23.5°	-18.6 dB	0.28%

More work on this topic has been done in relation directly to the HSX project. It will be discussed in Sec. E

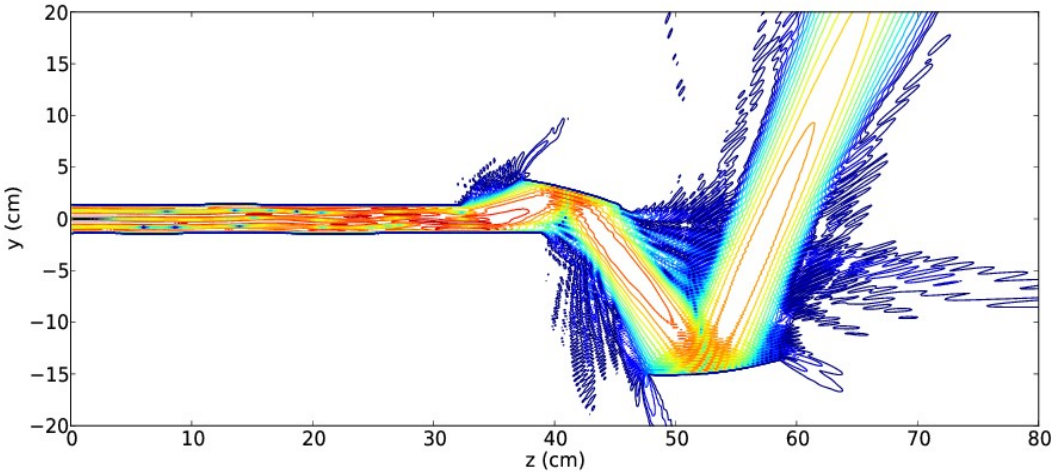

Fig. 12. Graph of E_y in a longitudinal plane for the complete two mirror 60 GHz converter system obtained from Surf3d.

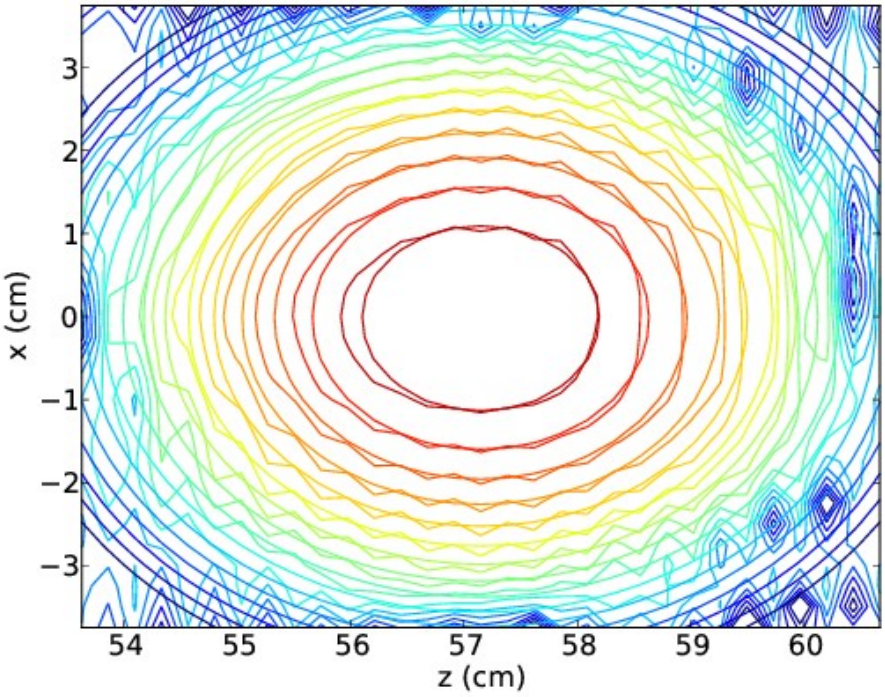

Fig. 13. Output of the total system, $|E_y|$ (dB) plotted on a tilted planar surface from Surf3d. The beam propagated through the system of Fig. 11 (wavy curves) is compared with the target Gaussian output beam.

D. Work on Traveling-Wave Resonator Design for High-Power Testing of Components (Bryan Fox)

D-1 Basic Concepts.

A cold test of the performance of high-power microwave components for high-power mm-wave transmission lines or mode converters is conventionally and simply done with low-power solid state sources such as Gunn oscillators. Unfortunately, the difficulties which may arise in a high-power (1-2 MW) system are not always apparent from a cold test. Testing components in such a high-power system requires a high-power gyrotron and a high-power power supply both of which are extremely expensive. Thus, it would be desirable to be able to test components at the power at which they will be used with a lower-power gyrotron.

A solution to this problem proposed by Tim Bigelow at ORNL is to use a traveling wave resonator, sometimes called a ring resonator. By constructive interference of multiple low-power beams such a resonator can create a much higher power traveling-wave beam. A simple ring resonator using a diffraction grating and three mirrors is depicted in Fig. 14. The operating principles of such a device are similar to the usual waveguide ring resonators [27]. Ideally, the diffraction plate would perform as a matched, reciprocal directional coupler with ports 1 and 4, and ports 2 and 3 decoupled.

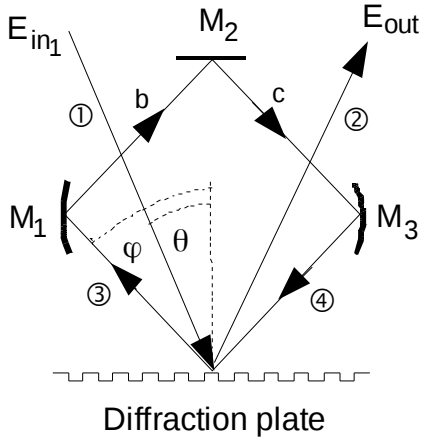

Fig. 14. Traveling wave resonator with two internal shaping mirrors.

As is well known, a grating plate can be made to split an incoming beam (say into port 1) into a spectrally reflected beam (port 2) and a diffracted beam (port 3). If the power from the diffracted beam is routed back into the system (through port 4), then we have a strong candidate for the main component of a microwave ring resonator which can produce high power in the circuit from port 3 to 4. In order for this resonance to occur a small adjustment must be made in the position of one of the mirrors in the ring (or more simply in the frequency) so that the phase of the input beam to port 4 is such that it reinforces the beam coupled from port 1. The circulating power in the closed "ring" could be more than ten times the input power depending on the loss in the ring and the coupling from port 1 to port 3 [27]. The resonator form depicted in Fig. 14 is for free space propagation. The form appropriate for Tim Bigelow to use would use path b and/or c as corrugated waveguides with components inserted. We will investigate the free space version of this at low power to test the basic function of the diffraction grating in a ring

resonator. Ben Rock began work on this project with a study of the deformation caused in a Gaussian beam by diffraction from a grating plate [28] (see Fig. 15).

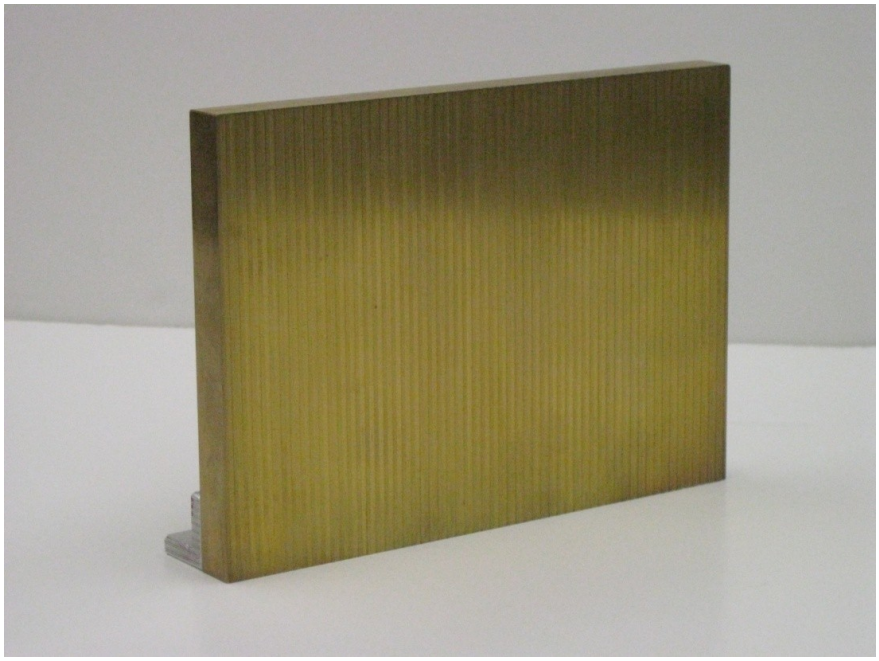

Fig. 15. Diffraction plate used in Ben Rock's experiments.

The resonator form shown in Fig. 14 is for the case where there is only one diffracted beam. In the high power version of the ring, it will be important only to have just one diffracted beam. In the low power version, it may be useful to have a second diffracted beam to facilitate testing. We will only consider the case of a design for one diffracted beam at present.

D-2 Design of Input Mirrors

If the input beam, E_{in1} in Fig. 14, is circular, which would probably be the case, then the diffracted beam would be elliptical. It would almost certainly be desirable to have the diffracted beam and the beam circulating in the resonator be circular. Thus, we have investigated placing one or two mirrors before the input to the resonator to make the input beam elliptical such that the diffracted beam and the circulating beam will be circular. This is shown in Fig. 16 for the case of two input mirrors and Fig. 17 for a single input mirror. Bryan Fox has done a design of a pair of mirrors for this purpose. Their surfaces are shown in Figs. 18 and 19. The complex coupling to the desired elliptical Gaussian beam is 99.6%. The exact position of the mirror pair relative to the resonator is not critical in that a good design can be found for different positions of the mirror pair.

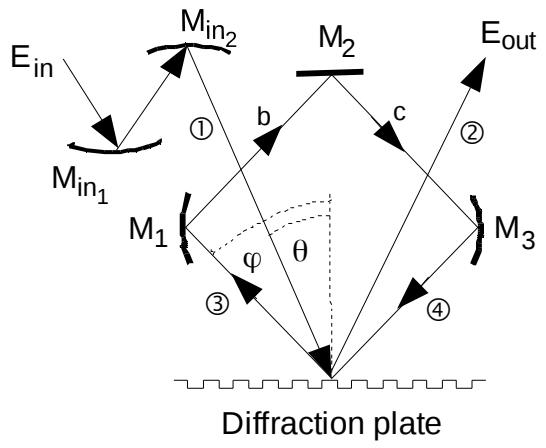

Fig. 16. Traveling wave resonator with two internal shaping mirrors and two input mirrors.

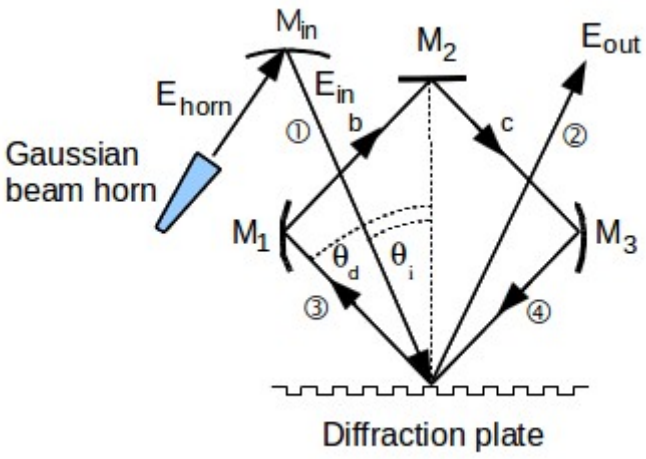

Fig. 17. Traveling wave resonator with two internal shaping mirrors and one input mirror. A Gaussian beam input horn is also shown.

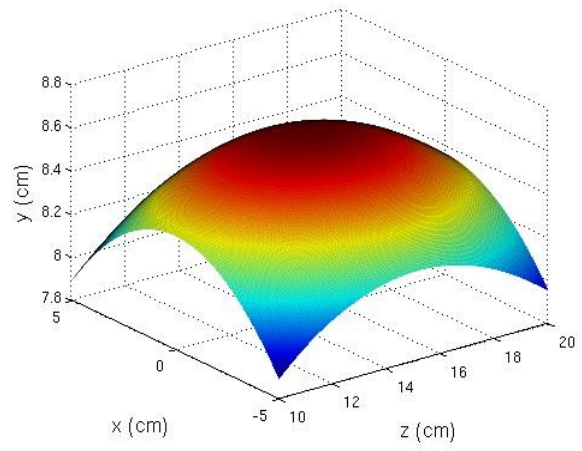

Fig. 18. Surface of M1 of the mirror pair designed to achieve the desired ellipticity of the input beam. Note that the vertical scale is much smaller than the either of the horizontal ones.

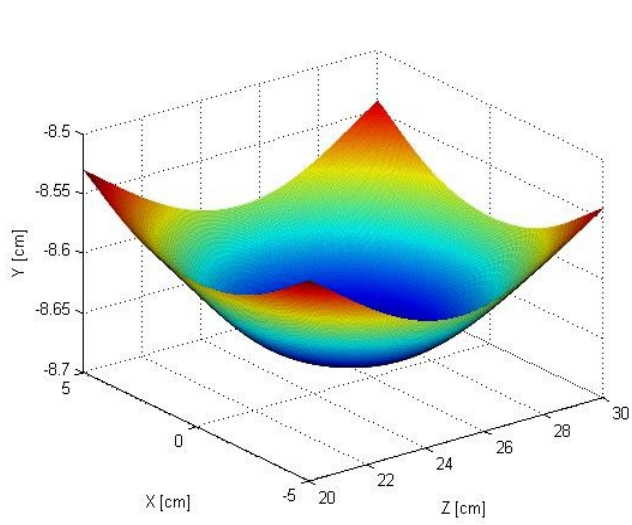

Fig. 19. M2 of the mirror pair designed to achieve the desired ellipticity of the input beam. Note that the vertical scale is much smaller than the either of the horizontal ones.

If the desired ellipticity is not too great, which is the case here, a single shaped mirror can be designed to obtain almost as good a result. An example of such a mirror is shown in Fig. 20. Figure 21 shows the comparison of the input ellipticities obtained for varying beam waists sizes in the y-direction for a constant waist of 2 cm in the x-direction for a two-mirror system and a

single mirror. For the input angles and diffracted beam angles that we will use, the desired value of the y-waist is approximately 2.3-2.4 cm where the single mirror case is still relatively good. Thus we anticipate using only a single input mirror since the improvement from adding the second mirror does not warrant the additional complication.

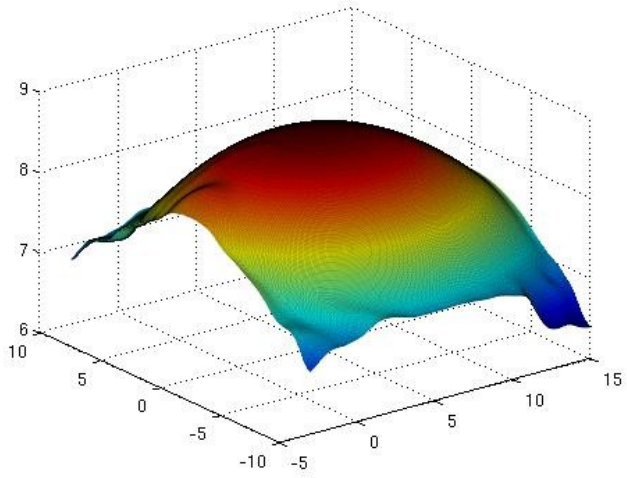

Fig. 20. Single mirror designed to achieve the desired ellipticity of the input beam. Note that the vertical scale is smaller than the either of the horizontal ones.

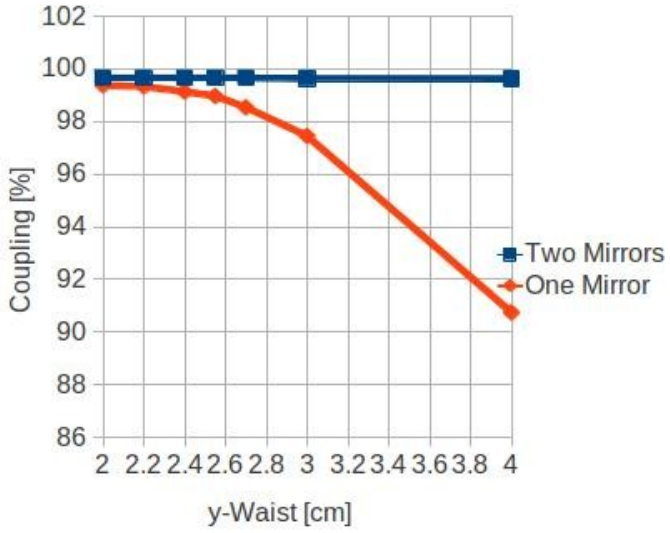

Fig. 21. Comparison of the complex coupling obtained for a two-mirror system and a single mirror system to convert the input ellipticity to the resonator from circular to elliptical for various y-waists. The waist in the x-direction is constant at 2 cm.

Figure 22 shows the traveling-wave resonator with mirror M_2 replaced by two sections of corrugated waveguide and a miter bend in a configuration that might be used to test these components

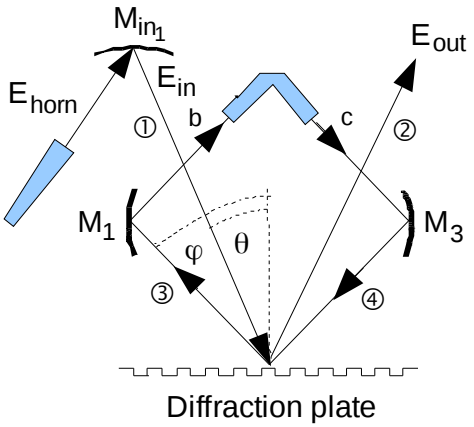

Fig. 22. Traveling wave resonator with two sections of waveguide and miter bend inserted in place of M_2 for testing.

D-3. Computations and Simulations

The power increase factor is the ratio of the power circulating in the resonator to the input power. It is also known as the power multiplication factor. Figures 23 and 24 show the power increase factor for varying ring attenuation and coupling to the diffracted beam. The losses in the system are very import in determining the power increase factor. These losses are ohmic loss and spillover loss plus an additional loss term in the simulation which is the mesh leakage loss. This is not a physical loss but only occurs in simulation. It can become significant if the mesh is not fine enough. However, this could be the case here if the simulation includes four mirrors and the diffraction plate which will need a substantial computation time. This computation time can be reduced if the mesh is made courser.

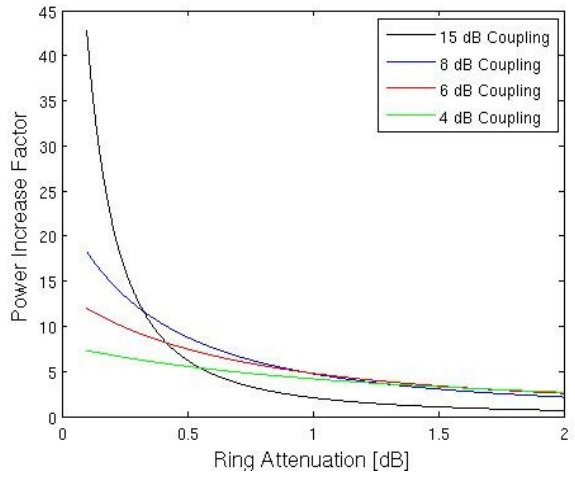

Fig. 23. Power increase factor in the resonator as a function of ring attenuation for several different coupling factors.

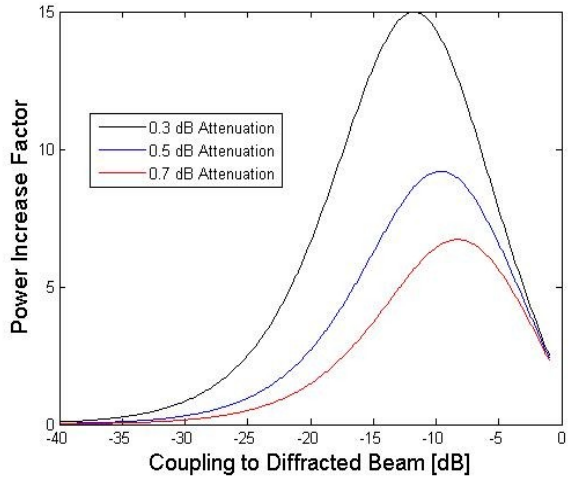

Fig. 24. Power increase factor in the resonator as a function of coupling factor for several different ring attenuations.

Figure 25 shows the increase in sensitivity of the power increase factor to mirror position (or frequency) for different couplings to the diffracted beam. From Figs. 23, 24 and 25 we conclude that a beam coupling of 4-6 dB may be best to avoid extreme sensitivity to mirror position, frequency and resonator attenuation.

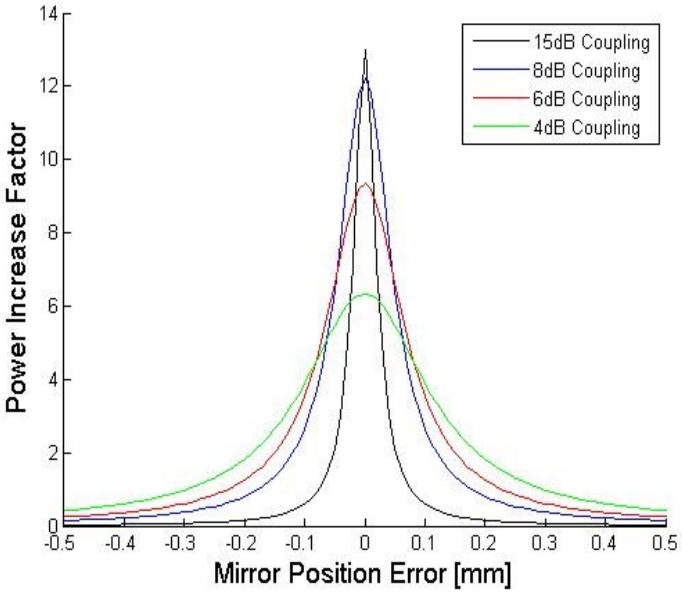

Fig. 25. Power increase factor versus the position error of one mirror for several coupling factors.

D-4. Simulations Using Surf3D

Tim Bigelow has sent us a diffraction plate which he will be unable to use, but has about the correct parameters for our test. The details of the corrugations are shown in Fig. 26. From Fig. 27, the coupling is found to be -6.6 dB. This diffraction plate will be used as the basis for all further computations in this section.

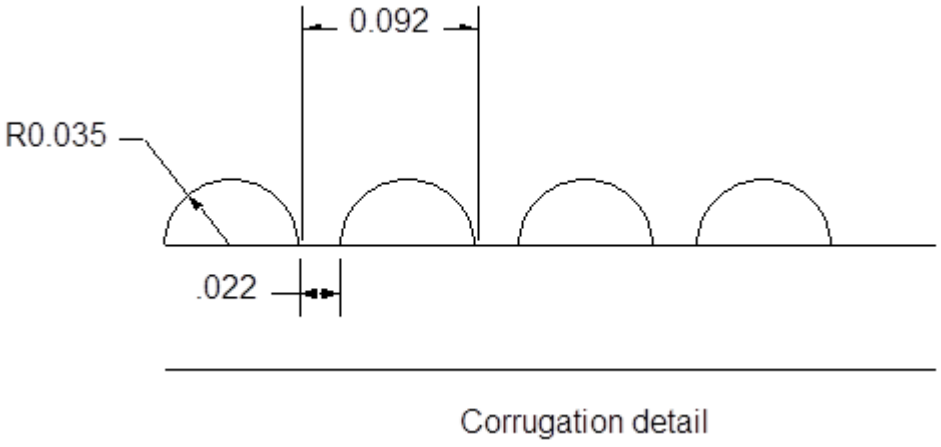

Fig. 26. Corrugation detail of the diffraction plate sent to us by Tim Bigelow.

Simulations were made using Surf3d for the Bigelow diffraction plate and the mirrors designed.

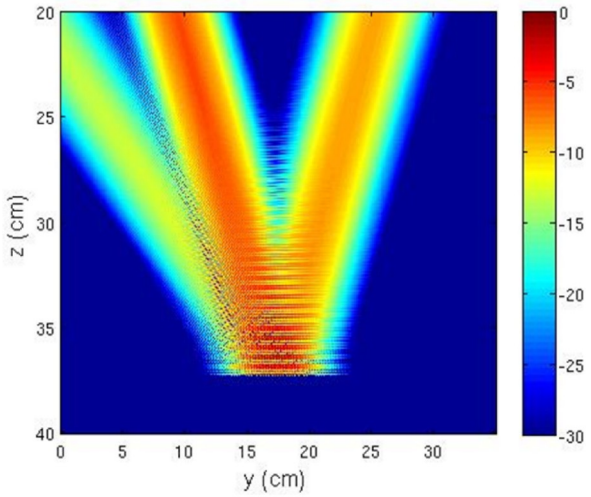

Fig. 27. Paths of the incident, specularly reflected and diffracted beams for a Gaussian beam incident on the Bigelow diffraction plate. The color scale is in dB.

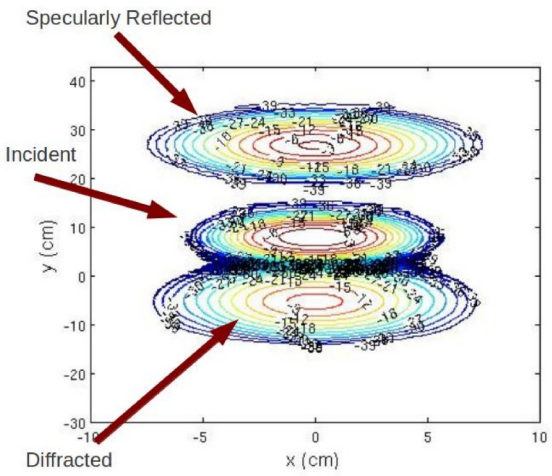

Fig. 28. Beam cross sectional patterns for the incident, specularly reflected and diffracted beams for a Gaussian beam incident on the Bigelow diffraction plate. The contours are from -3 dB to
-39 dB in 3 dB increments.

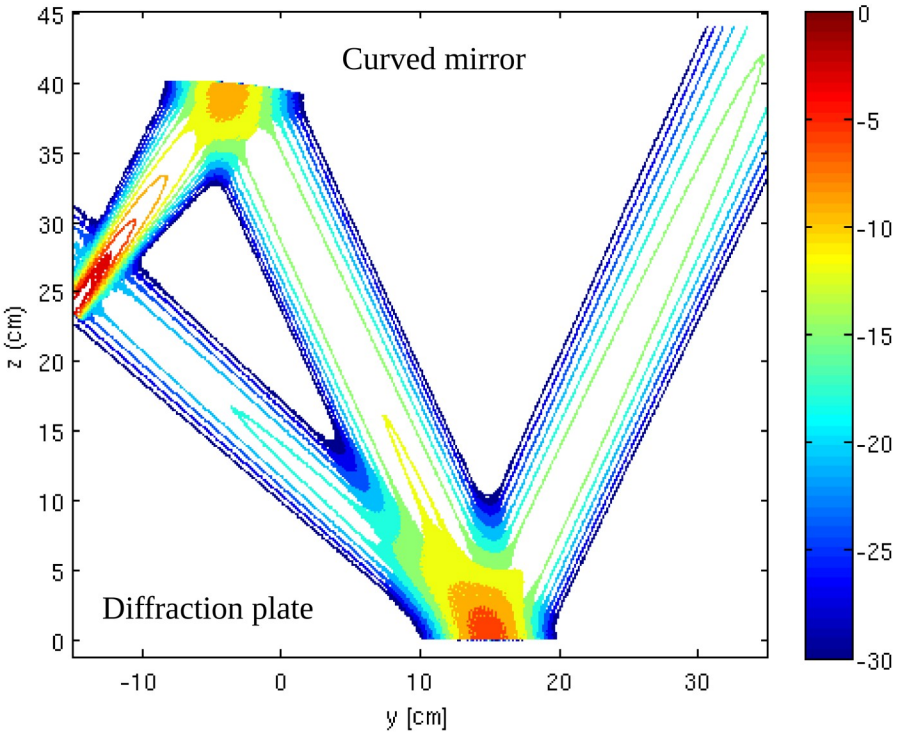

Figure 29. Surf3d simulation of a Gaussian beam injected into the input mirror and grating in the y - z plane with x = 0. The color scale is in dB.

In addition to the input mirror (to obtain the correct input ellipticity) the two curved resonator mirrors were also designed. The design was tested in simulation as shown in the complete TWR simulation result shown in Fig. 28 below.

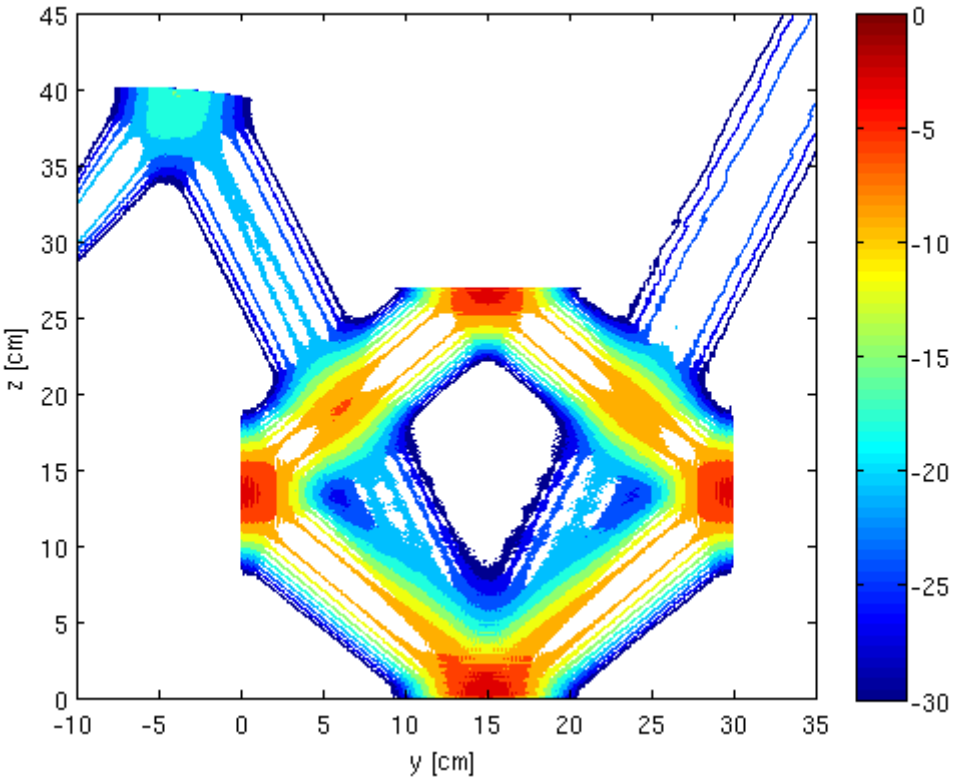

Fig. 30. Result of Surf3d simulation of a TWR shown in the y - z plane with x = 0. The simulation is for a resonator 20.2 cm on a side with 6.6 dB coupling, 0.03 dB attenuation and a frequency of 110 GHz. The color scale is in dB.

D-4. Simple Model for the Power Inside the Resonator

If we have a beam with amplitude 1 input into the TWR, the amplitude of the wave inside the resonator will grow to

$$1+x+x^2+\ldots=\frac{1}{1-x} \qquad \text{(D.1)}$$

where x is the amplitude of the wave after one complete circuit having incurred coupling losses, spill over and ohmic attenuation. In general x will be complex, accounting for the phase, q, incurred through the resonator,

$$q = k\ell + 4 \arctan(\ell/4b) + \varphi_r \ , \qquad \text{(D.2)}$$

where k is the free space wave number, *l* is the total length around the resonator, $b = \pi w_0^2/\lambda$ is the confocal parameter, and φ_r accounts for the phase shift from the difraction grating and off-axis reflection from the mirrors.
The phase shift due to the off-axis reflection from the internal refocusing mirrors was carefully studied by simulation with Surf3d. It was found to be only 2.5° (in addition to the 180° phase shift due to the refection from a good conductor.) The phase shift due to the refletion and diffraction from the diffraction plate plate was also carefully studied. The results are very interesting and complex. The phase shift depends on exactly where the reference plane for the phase is chosen to be. It is discussed in Sec. D-5 below and more fully in Fox's dissertation [30].

The power increase factor as a function of frequency for the simple theory is compared with results from the simulation in Fig. 31 for the parameters of the resonator. The agreement is excellent. Establishing the validity of the simple theory is important because it can be used to predict the behavior of the resonator.

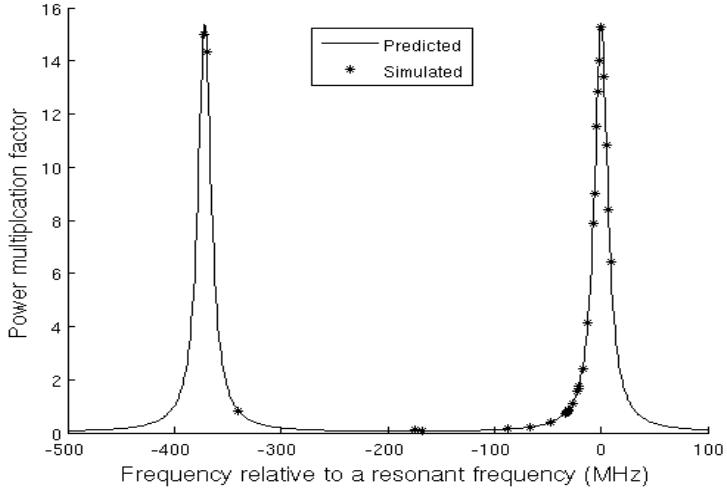

Fig. 31. Power in TWR vs. frequency calculated with Eq. (1) (solid line) with Surf3d simulated points denoted by * .

The resonant frequencies for a TWR can be found from

$$f_{res} = \frac{c}{l}\left(p + \frac{2}{\pi}\arctan\left(\frac{l}{4b}\right) + \frac{\varphi_r}{2\pi}\right) \qquad \text{(D.3)}$$

where p is an integer.

The resonator power as a function of frequency was also obtained for the TEM_{10}, TEM_{01} and TEM_{11} modes from simple theory and simulations. The results are plotted in Fig. 32. The results were the same for the TEM_{10} and TEM_{01} modes. It is important that these higher order modes do not have the same resonant frequencies as the TEM_{00} mode. Thus, the higher order modes that are created in the resonator, say by microwave components under test will not

resonate and thus will not build up. This was studied in more depth by Bryan Fox and is presented in his dissertation. The phase term becomes

$$q = kl + 4(m + n + 1) \arctan(l/4b) + \varphi_r \ , \qquad (D.4)$$

where m and n are the modal indices.

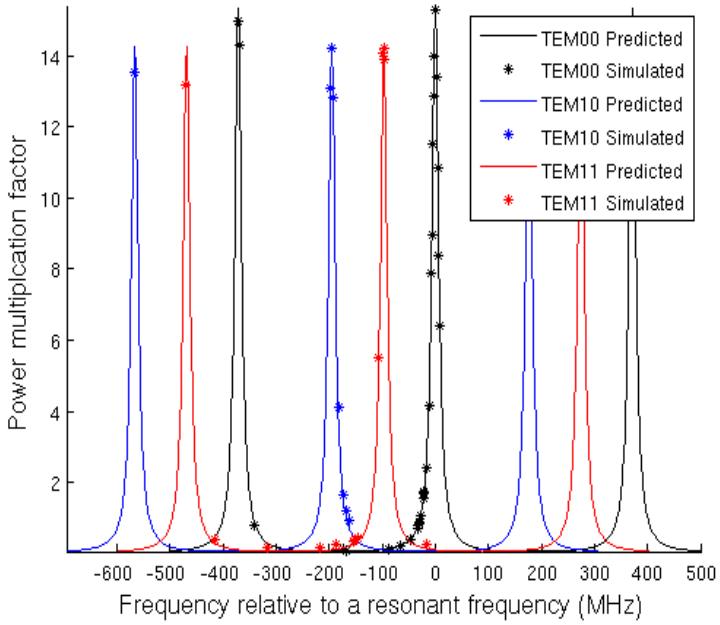

Fig. 32. Resonance of some higher-order modes in the TWR.

Fig. 33. shows the resonance of the TRW as the total length is increased from1 m to 2 m to 10 m. I can be seen that as the resonator length gets larger the resonance peaks becomes narrower and closer together. This is important because the resonator must remain "stable" for the frequency variations of the gyrotron. The following quotation from Kevin Felch of CPI [31] gives some information relevant to the required stability.

"In terms of short-term frequency stability, the expansion of the cavity dominates during the first 200-400 ms, where the frequency will drop by 100 MHz-300 MHz, depending on power level and operating frequency. By the time you reach pulse widths of around 1 second, the frequency becomes quite stable and changes in frequency are dominated by the voltage stability. I showed a spectrum analyzer video in our DOE meeting in 2012 where we looked at the stability of the VGT-8115 S/N 2 gyrotron over a 10-s pulse while operating at 500 kW output. The spectrum analyzer was set at 10 MHz per division so it appeared that after the first second, it was stable to within about 2 MHz with our power supply. For somewhat longer pulses you have to worry about the drop in beam current due to emission cooling which will lower the frequency as well by a few MHz, depending on how well you boost the filament to compensate for the emission cooling. Ultimately, by the time you reach more than one minute, I think you are just left with

power supply fluctuations, assuming the cooling water is controlled adequately. If there is a gradual increase in the cooling water temperature, that will also serve to decrease the frequency somewhat."

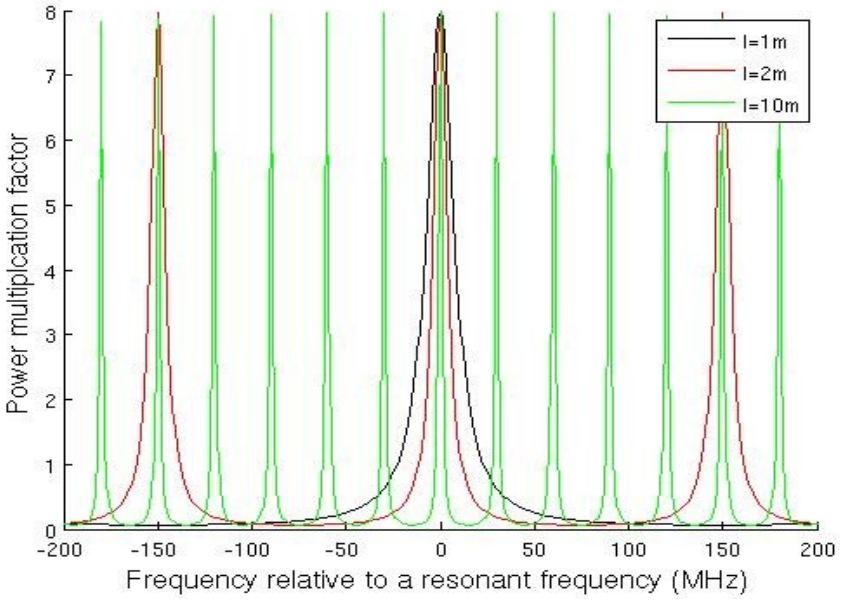

Fig. 33. Power multiplication factor as a function of frequency for different resonator lengths.

D-5. Phase Shift and Lateral Beam Displacement at the Diffraction Plate

A detailed simulation of a Gaussian beam incident on the diffraction plate (removed from the resonator) at the desired input angle was carried out using Surf3d. It was found that there was a small lateral shift in the reflected and diffracted beams depending on where the reference plane for the reflection was chosen. This is similar to what is predicted by the work of Zhang and Tamir [32]. Since we are most interested in the phase shift of the reflected beam, we chose the reference plane such that there was no lateral shift for that beam. (See Fig. 34 below.) Then the phase shift of the reflected beam (at an angle of 48.04°) was found relative to that plane to be about 15°. The lateral offset from incident beam to diffracted beam is 0.743 mm in the backward direction with respect to this plane.

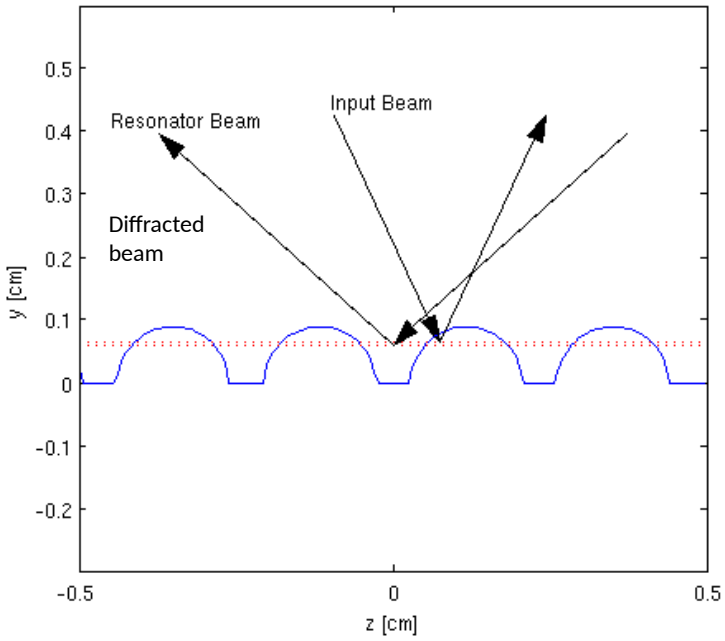

Fig. 34. Diffraction grating showing the lateral shift found in simulations. The arrows show the propagation directions of the beams. The dotted red line shows the reference plane chosen. The lateral offset from incidence beam to diffracted beam is 0.743 mm with respect to this pane.

D-6. Experimental Results

In order to build the complete resonator, an accurate alignment system would need to be fabricated as well because of the sensitivity of the resonator to small misalignments. Building this kind of alignment system would be prohibitively expensive for our budget, so instead only the input mirror and one of the resonator refocusing mirrors were fabricated and tested with the diffraction grating received from Bigelow. The only parts of the system that were not built then were the flat mirror and the other resonator refocusing mirror, aside from the alignment system. There is very little doubt that the second resonator mirror, which is the same as the first resonator mirror rotated 180°, would perform as well as the first.

The input mirror is shown in Fig. 35. It was tested with a circular beam from a Gaussian beam horn (shown in a later figure). Figure 36 shows a measurement taken at a plane perpendicular to the beam reflected from the mirror centered where the grating would be. The measured beam is off by about 1 cm in z at a distance of 44 cm from the mirror. This could be explained by the beam being off in angle by about 1.3°. If the total angular misalignment is 1.3°, the input mirror would only need to be tilted by 0.65°to correct for the misalignment, and we do not expect to be able to align components better than 1° without a total rigid alignment frame. Other than the slight misalignment, the comparison is very good. The desired ellipticity was obtained.

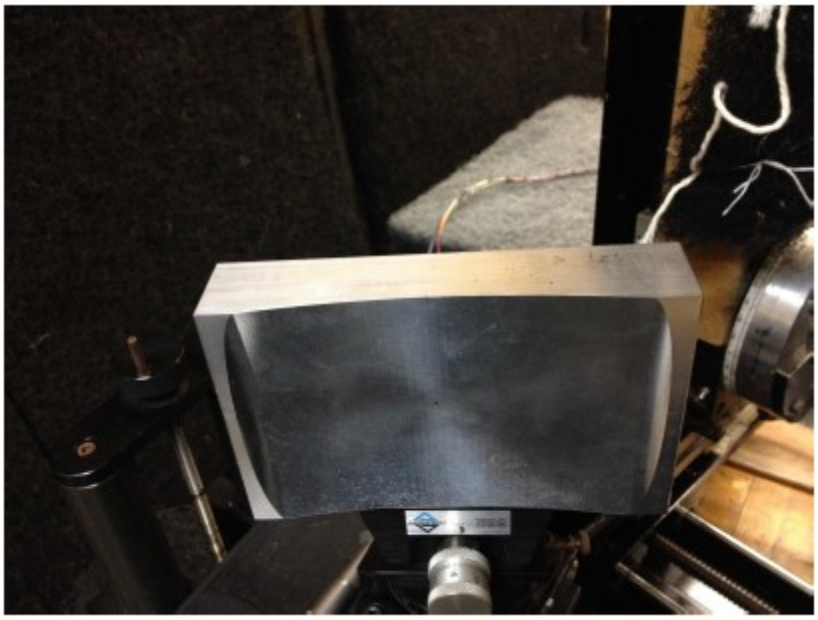

Fig. 35. Input mirror mounted on a series of positioners.

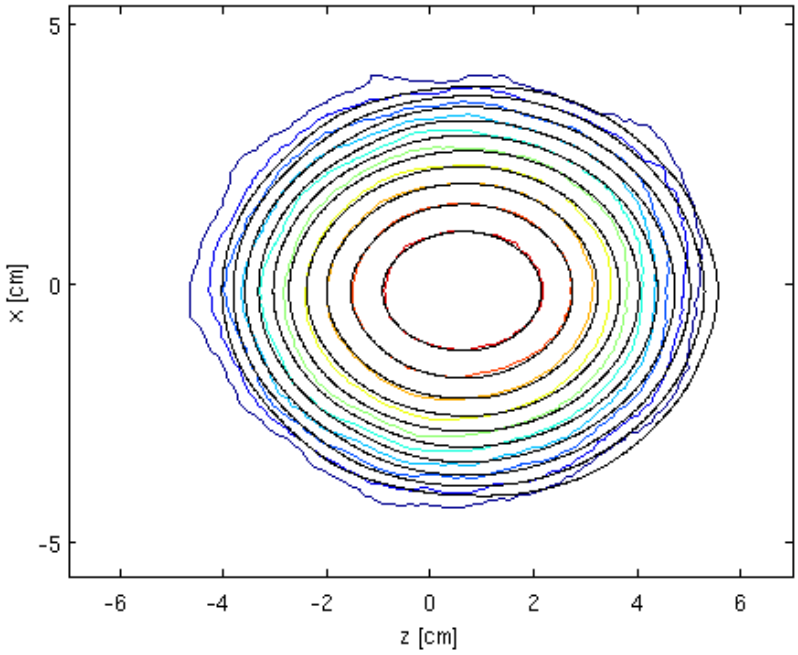

Fig. 36. Measured (color) and simulated (black) beam from input mirror at a plane centered at the center of the grating perpendicular to the direction of propagation. The contours are in 3 dB increments from -3 dB to -30 dB below the maximum power of the beam.

The diffraction plate is shown in Fig. 37 and the first resonator refocusing mirror is shown in Fig. 38. A set up was constructed which allowed the measurement of the refocused diffracted beam from the refocusing mirror and the reflected beam from the diffraction plate for one alignment set up. This set up is shown in Fig. 39.

Figure 40 shows the measured (color) and simulated (black) beam reflected from grating at angled plane perpendicular to the propagation direction of the *diffracted* beam after the refocusing mirror. Figure 41 shows the diffracted beam after it has been refocused with the first resonator mirror. Figure 41 is a comparison of the measured beam in color and the simulated beam in black, at a plane perpendicular to the direction of propagation, centered where mirror 2 would be located in the resonator. These measurements show excellent agreement with simulation and validate the design method for both mirrors.

Fig. 37. Grating from Bigelow.

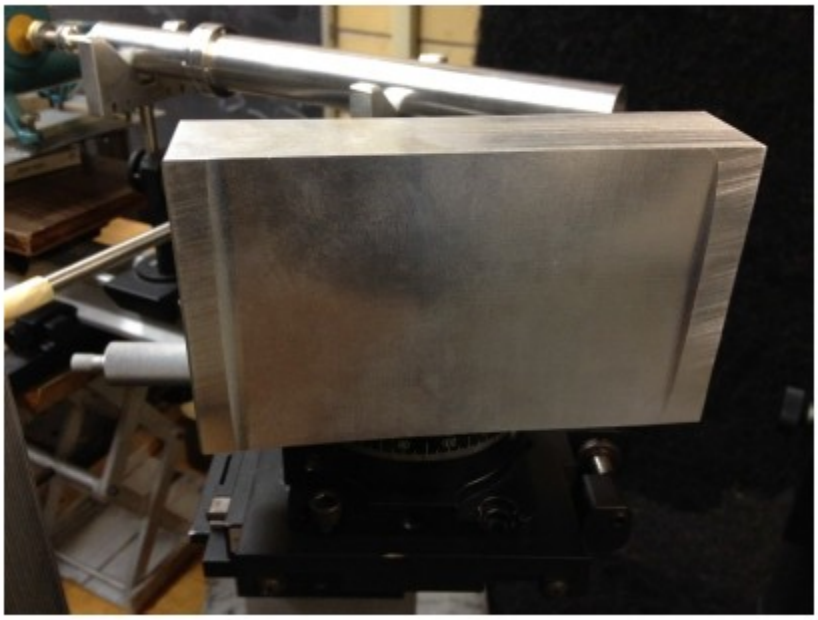

Fig. 38. Resonator refocusing mirror mounted on a series of positioners.

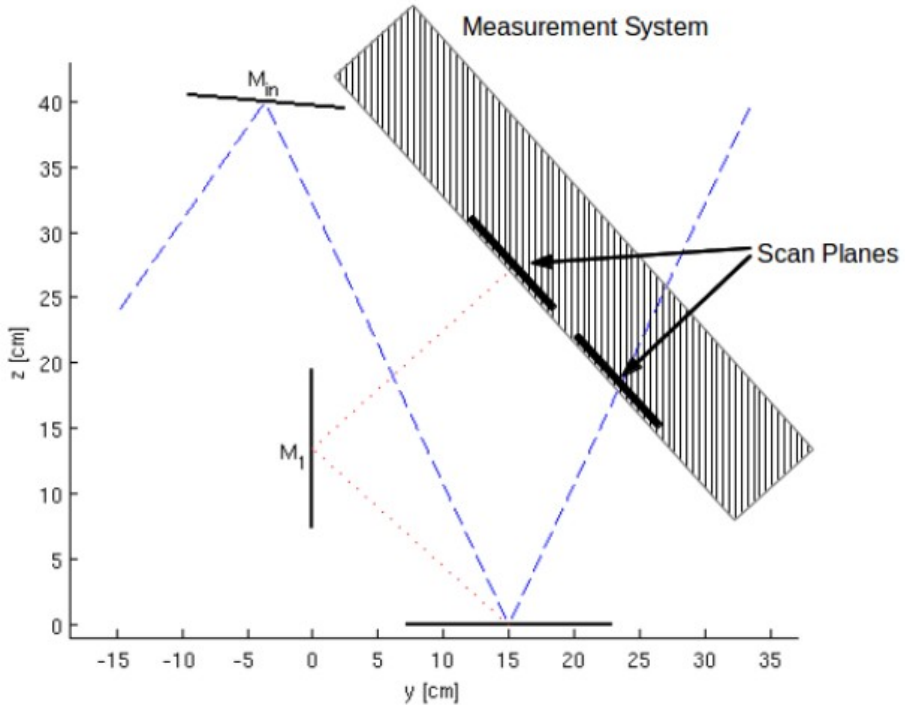

Fig. 39. Positioning of measurement system for grating and focusing mirror measurements.

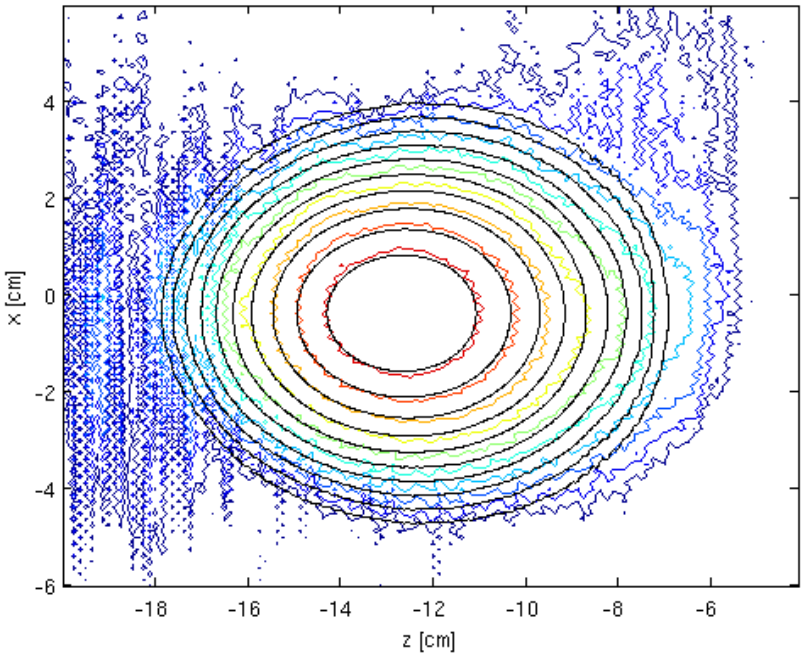

Fig. 40. Measured (color) and simulated (black) beam reflected from grating at angled plane perpendicular to the propagation direction of the *diffracted* beam after the refocusing mirror. The contours are in 3 dB increments from -3 dB to -30 dB below the maximum power of the beam.

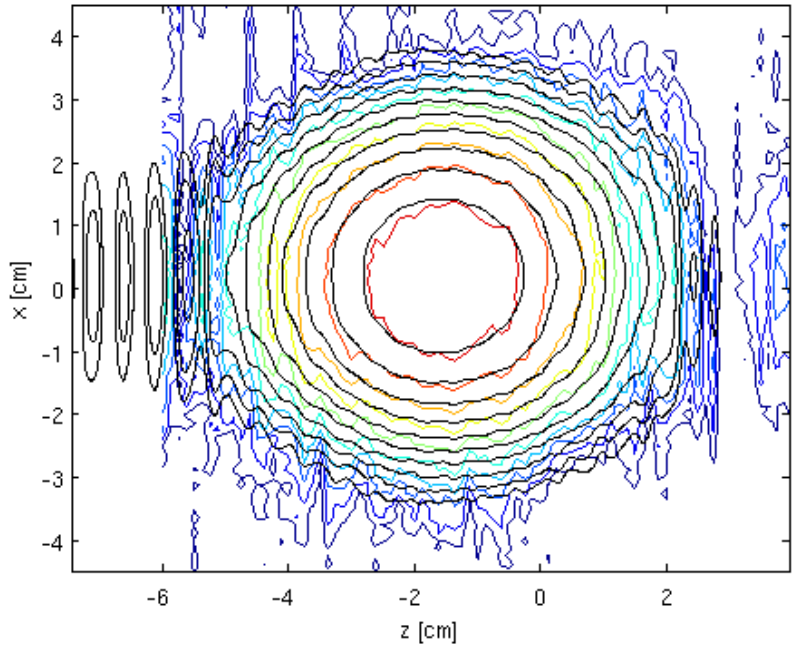

Fig. 41. Measured (color) and simulated (black) diffracted beam refocused by mirror 1 at plane centered at mirror 2 perpendicular to plane of propagation. The contours are in 3 dB increments from -3 dB to -30 dB below the maximum power of the beam.

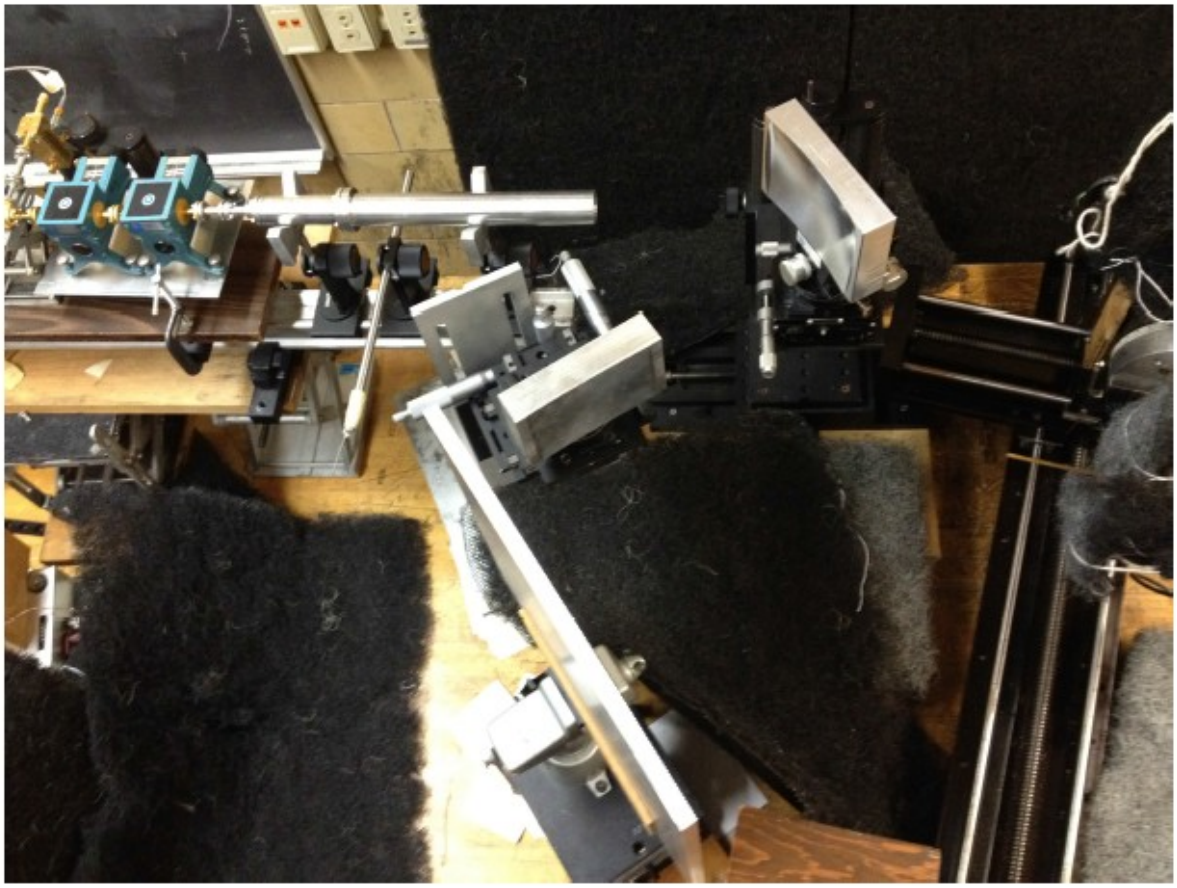

Fig. 42. Picture of the measurement system as well as the mirrors, grating and Gaussian beam horn in the anechoic chamber. The black foam material is absorber.

A copy of Fox's dissertation has been sent to Bigelow.

E. Investigating and Improving the HSX Microwave Transmission System (Eric Buscarino and Xiaodong Wang)

E-1. HSX Microwave Transmission System Past Design

HSX is a quasi-helically symmetric stellarator at the University of Wisconsin-Madison with a Varian 28 GHz TE_{02} gyrotron used for plasma heating and breakdown [33]. The microwave transmission system from the gyrotron to the plasma is shown in Fig. 43. Currently a smooth-wall Vlasov launcher, shown in Fig. 45, with a radius of 3.175 cm and a 2.66 ratio of operating frequency to cutoff frequency is used to feed a complex quasi-optical transmission line which feeds the stellarator. The original design of the transmission system was done using geometrical optics approximations which have some limitations.

Our goal in this part of the project was first to compare these design results with the more accurate Surf3D computational system, then to look for ways of improving the efficiency of the system by simple methods and then by considering a perturbed-wall launcher.

Although the output from the perturbed-wall launcher has increased Gaussian content and improved directivity, the current HSX system was designed for the smooth-wall Vlasov launcher so we expect that system design changes would be necessary to make use of the improved output from the perturbed-wall launcher.

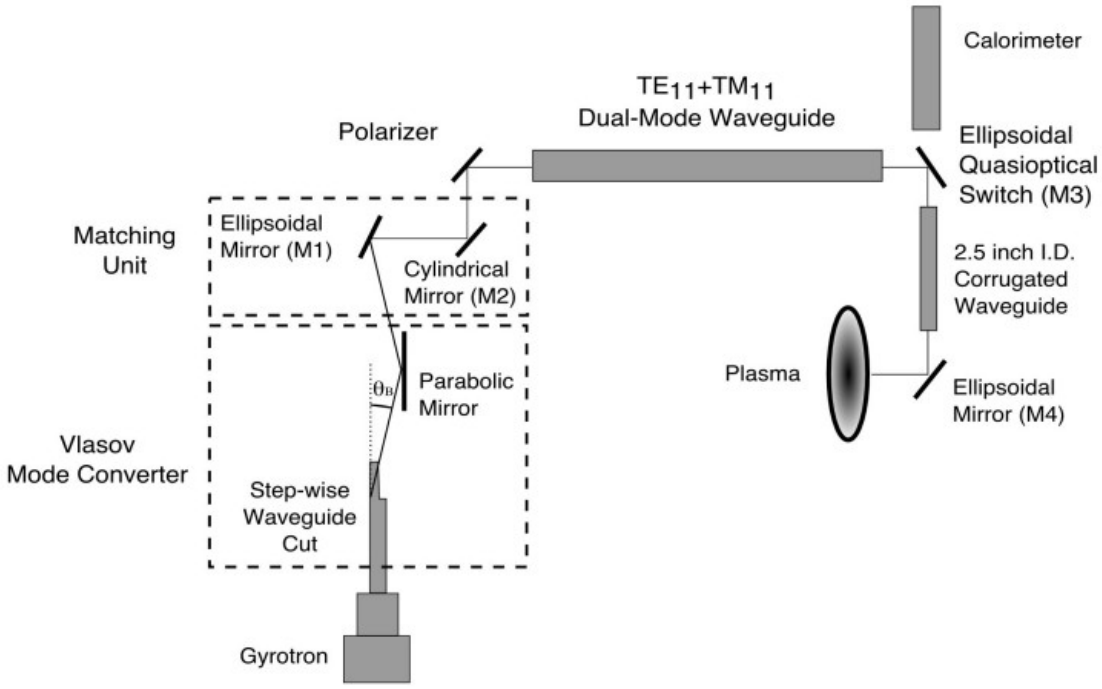

Fig. 43. Schematic diagram of the transmission system for plasma heating in the HSX Stellarator.

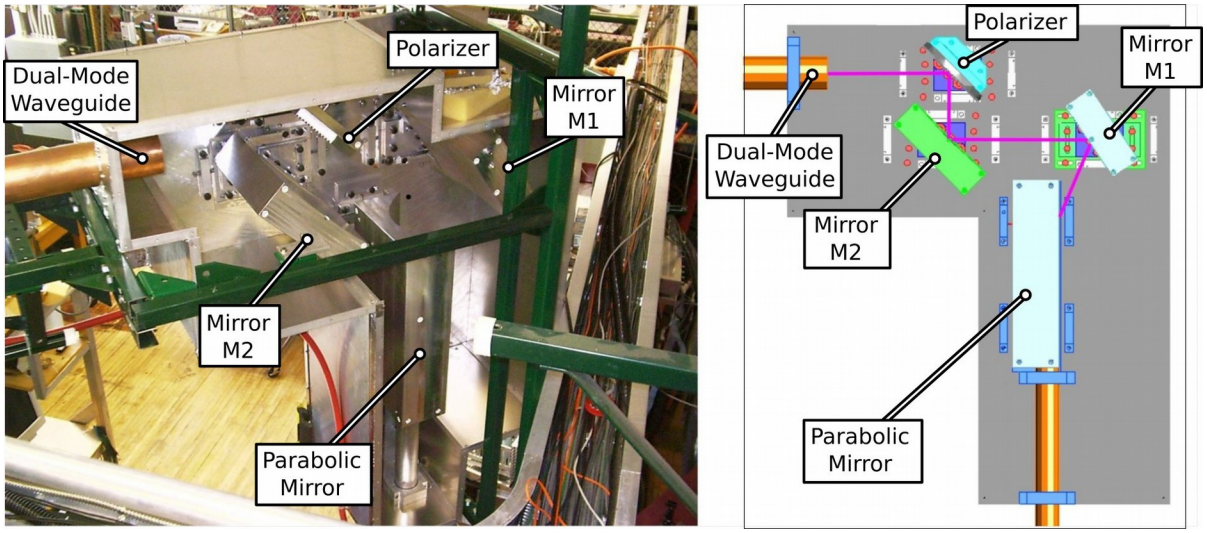

Fig. 44. Transmission system for plasma heating in the HSX Stellarator.

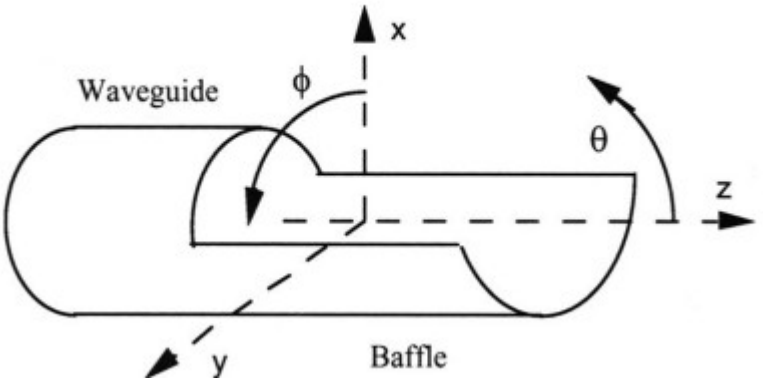

Fig. 45. Generic drawing of a TE_{0n} launcher with the corresponding coordinate system.

The HSX transmission system consists of five design units: a quasi-optical TE_{02}-to-TEM_{00} mode converter, a matching unit, a polarizer, a dual-mode (TE_{11}+TM_{11}) waveguide, and a quasi-optical switch. The following work simulated the first three units of the system and focused on the input to the dual-mode waveguide. The HSX microwave transmission mirrors were designed for the system using a quasi-optical design technique. Small but significant amounts of other TE_{0n} modes are produced by the gyrotron, but are not expected to propagate through the system due to the fact that their launcher output angles are different from the TE_{02} mode.

E-2. Geometrical Optics Theory

Inside the launcher waveguide the fields can be pictured as waves propagating down and bouncing off the walls inside of the waveguide. The geometrical optics of circular waveguides uses the properties of Bessel functions. The Bessel function of the first kind, J_m , can be written as

$$J_m(x) = \frac{H_m^{(1)}(x) + H_m^{(2)}(x)}{2} \qquad \text{(E.1)}$$

where $H_m^{(1)}(x)$ and $H_m^{(2)}(x)$ are the Hankel functions of the first and second kind respectively.

For TE_{0n} modes m = 0. For propagation in the +z direction, the mode generating field, H_z, and is given by

$$H_z^{+}(\rho,\phi,z) = J_0(\beta_\rho \rho) e^{-j\beta_z z} \quad . \tag{E.2}$$

For TE_{0n} modes, under the geometrical optics approximation

$$H_0^{(1),(2)}(x) \approx \sqrt{\frac{2}{\pi x}} e^{j(\pm x \mp \pi/4)} \tag{E.3}$$

for large x. From Eq. (E.3) only the phase components are of interest and the phase correction is close to the exact value as can be seen in Fig. 46. In Eqs. E.1-E.3, x is a dummy variable that is replaced with $\beta_\rho \rho$ where $\beta_\rho \rho = \chi'_{mn}\left(\frac{\rho}{a}\right)$.

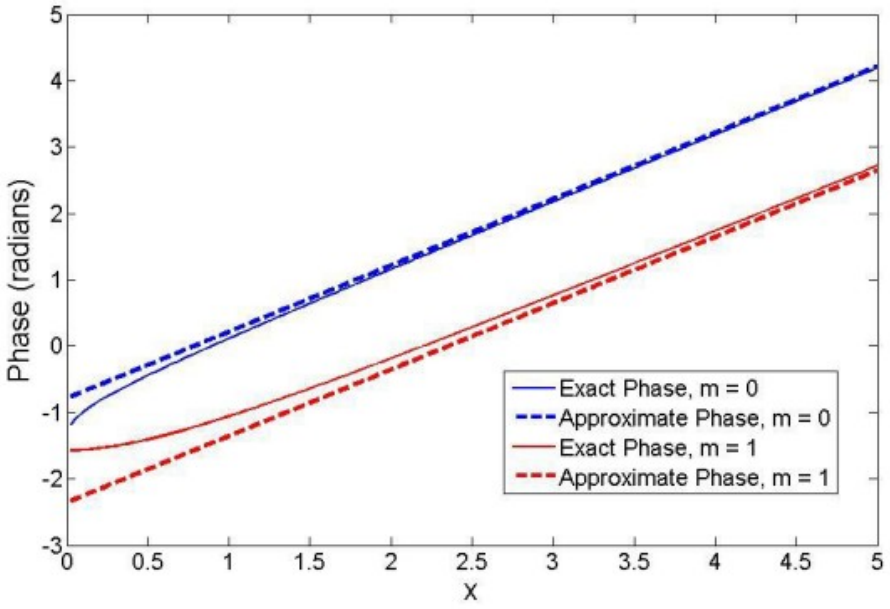

Fig. 46. Comparison between the phase values of the approximation of $H_m^{(1)}$ in Eq. (E.3) and the exact value of $H_m^{(1)}(x)$ for m = 0 and m = 1.

If Eq. (E.1) and (E.3) are inserted into Eq. (E.2) the phase component of the field becomes

$$+¿(\rho,\phi,z)$$
$$H_z^{¿}$$
$$¿$$
$$arg\,¿$$
. (E.4)

where its gradient is

$$+¿(\rho,\phi,z)$$
$$H_z^{¿}$$
$$arg(¿)\approx-\beta_\rho\hat{\rho}-\beta_z\hat{z}$$
$$N(\rho,\phi,z)\approx\nabla\,¿$$
. (E.5)

Locally normal to the surfaces of constant phase can be visualized as a continuous beam of rays where the gradient of the wave front represents the direction of the rays. This is shown in Fig. 47. From this it can be seen that the rays propagate at a fixed angle to the waveguide axis in the waveguide axis plane. This fixed angle is known as the axial bounce angle, θ_b, and is given by

$$\cos(\theta_b)=\frac{N(a,\phi,z)\cdot\hat{z}}{|N(a,\phi,z)||\hat{z}|}=\frac{\beta_z}{\sqrt{\beta_\rho{}^2+\beta_z{}^2}}=\frac{\beta_z}{\beta}\quad,$$ (E.6)

For a radial cross section of the waveguide, it can be seen that the component of ray propagation parallel to the transverse plane is entirely in the radial direction.

$$N_t(a,\phi,z)\approx\frac{\chi'_{02}}{a}\hat{\rho}$$

For a given waveguide with fields operating at a set frequency, the axial bounce angle, θ_b increases for each higher order TE_{0n} mode. This allowed the HSX system to be designed specifically for the TE_{02} mode and creates a situation where higher and lower ordered modes cannot propagate through the system. In addition to the bounce angle increase with higher order TE_{0n} modes, the bounce angle also decreases with frequency, *f*. This results in θ_b becoming smaller the further a mode operates above the cutoff frequency, f_c, and getting larger as a mode operates closer to the cutoff frequency. In the former case θ_b approaches 0˚ as the f approaches infinity and θ_b approaches 90˚ as f approaches f_c. A parameter called the oversize factor indicates how far a mode operates from the cutoff frequency

$$OF = \frac{f}{f_c} = csc\,\theta_b \quad .$$

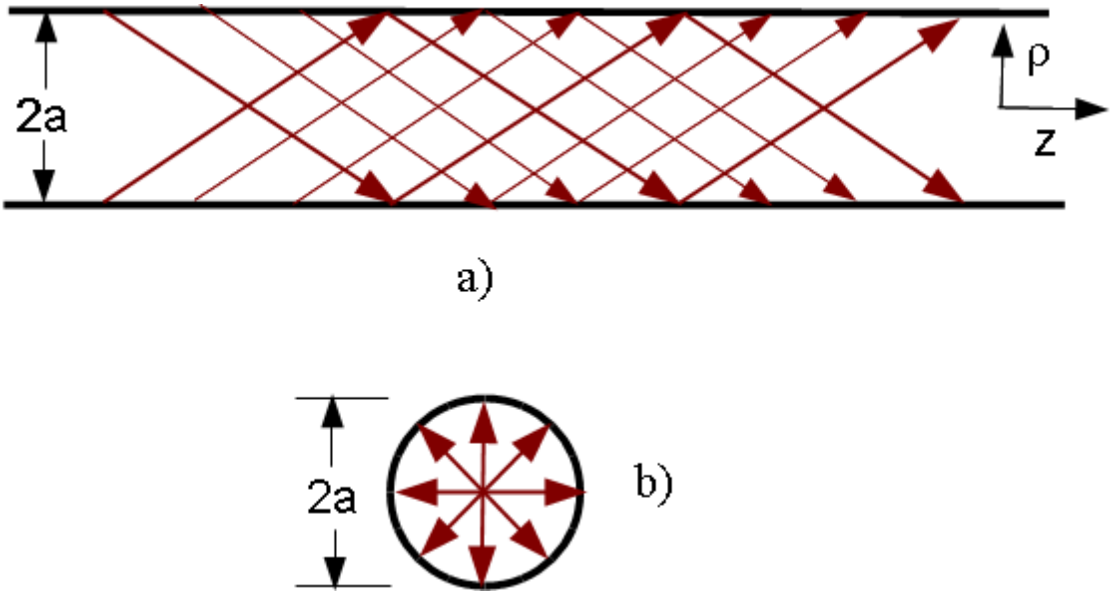

Fig. 47. Rays of a general TE_{0n} mode propagating inside a waveguide by bouncing along the waveguide walls, with the arrows representing the propagation direction. a) Schematic representation of the side view (a waveguide axis plane) of a generalized TE_{0n} mode. b) Radial cross-section of a generalized TE_{0n} mode.

The rays' behavior described in the preceding paragraphs show that all the rays completely bounce off segments of the waveguide walls. These segments of waveguide wall are referred to as Brillouin zones. These zones are periodic and form rectangles when unrolled onto a planar surface as shown in Fig. 48. Brillouin zones are not unique and performing a longitudinal translation or a rotation on a Brillouin zone will yield another Brillouin zone. An analogous description of Brillouin zones is as a set of cylindrical mirrors that reflect and propagate beams. It is important to note that these cylindrical mirrors border one another without overlapping and therefore form a complete circular waveguide. It can be seen that by removing one Brillouin zone from a circular waveguide that, according to this simple model, all of the fields exit through this hole and no fields will further propagate in the waveguide. Of course this is an idealized case and does not take into account diffraction. For the Vlasov launcher the last Brillouin zone at the end of the waveguide is removed so that the fields and power are propagated into free space. The output radiation patterns of Vlasov launchers are difficult to work with and often perturbations on the waveguide walls and/or outside mirrors are needed to improve the radiation pattern. Fig. 49 shows the side view of a TE_{0n} launcher.

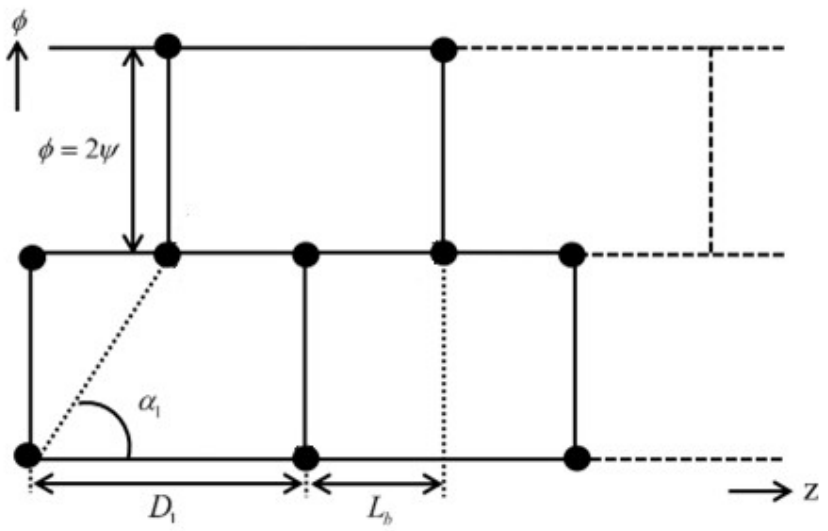

Fig. 48. Unrolled Brillouin zones for different TE modes. Broken lines indicate regions to be excised in a Vlasov launcher. Black dots trace out the rays bouncing location on the walls, where 2ψ is exactly 180˚, and $2D_1/L_b$ is exactly to 2.

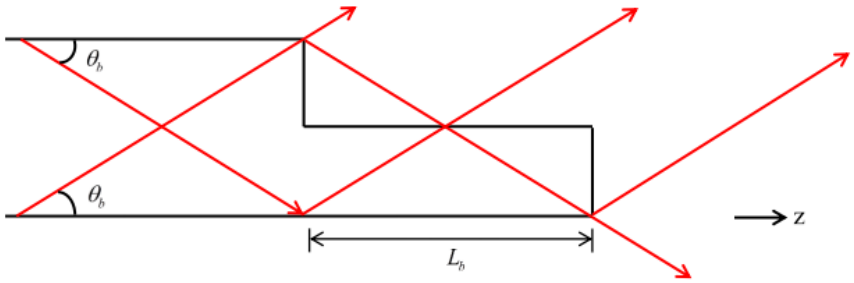

Fig. 49. Schematic representation of the side view of a rectangular-cut TE_{02} (non-rotating mode) launcher. Red arrows indicate propagating rays in or exiting the launchers.

The Vlasov mode converter was designed to convert the TE_{02} gyrotron output to a TEM_{00} Gaussian microwave beam. If the radius of the waveguide is given by a, then the bounce angle θ_b, and bounce length L_B are defined by

$$\theta_b = \sin^{-1}\frac{\beta_\rho}{\beta}$$

$$L_B = 2a\cot\theta_b$$

$$\beta_\rho = \chi'_{0n} / a \left(TE_{0n} modes \right)$$

where k is the free space wavenumber and χ_{mn} and χ'_{mn} are the nth zeroes of $J_m(x)$ and $J'_m(x)$ respectively, the Bessel function of the first kind and its derivative. For the TE_{02} mode for a waveguide with $a = 3.175$ cm and a system frequency of 28 GHz, the values of these variables are $\theta_b = 22.1°$, and $L_B = 15.63$ cm. The mode converter was implemented by using a step-wise cut wave guide and a parabolic mirror placed at the focal distance, $F = 6.1$ cm, above the center of the waveguide as can be seen in Fig. 50.

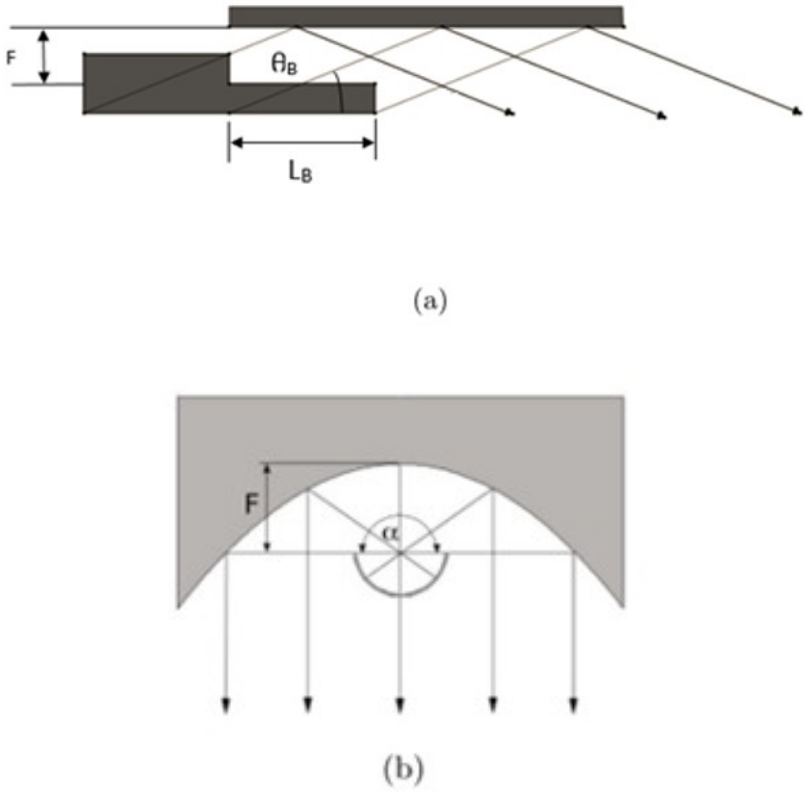

Fig. 50. Vlasov converter: a) side view b) end view.

E-2. HSX Microwave Transmission System Simulation

The HSX transmission line system up to the TE_{11}+TM_{11} dual-mode waveguide was analyzed using Surf3d simulation software. Surf3d is a method-of-moments program created by Jeff Neilson at Lexam Research for calculating the electromagnetic field scattered from metal surfaces. This section of the HSX system was chosen for analysis because the output of the Vlasov launcher is transformed and the most opportunity for power loss and possible improvement takes place within the Vlasov mode converter and the matching unit. An aspect of the system that was simplified was the polarizer that exists between M2 and the dual-mode waveguide. The polarizer was replaced with a simple planar mirror of similar geometry. It was assumed that minimal power loss takes place once the beam is input into the dual-mode waveguide.

It is evident that, while the geometrical design of the system is suitable, an improved system could be implemented using a perturbed-wall launcher. We expected the majority of power loss to take place initially from output of the Vlasov launcher and from the beam input to the waveguide. In addition to these two main factors it was also important to determine the amount of power lost due to spillover at M1, M2, and the polarizer.

At the input to the dual-mode wave guide it was important to consider two main factors, the total power in the beam and the Gaussian content of the beam. The total power in the beam was calculated by

$$P = \iint_A S \cdot d\,A \qquad \text{(E.12)}$$

where A is simply the cross-sectional area of the dual-mode waveguide and S is the power density of the beam at the start of the waveguide given by

$$S = \frac{1}{2}\Re\{E \times H^{i}\} \quad .$$

The Gaussian content of the beam was calculated through the power coupling coefficient c_p given by

$$c_p = \frac{\left|\iint E^{i}(u) f(u)\, du\right|^2}{\iint |E(u)|^2 du \iint |f(u)|^2 du}$$

A Gaussian beam is a close approximation to what is needed as an input to the dual-mode waveguide.

Using Surf3d we were able to propagate the beam from the launcher to the dual-mode waveguide input. A 28 GHz TE_{02} incident field was input at the start of the launcher. The overall

profile of the resulting beam propagating through the system is shown in Fig. 51. From this simulation we were able to find the incident power at the entrance to the dual-mode waveguide to be 79.15% of the initial power and the Gaussian power coupling coefficient to be 0.9273 giving a 73.4% power coupling to the target Gaussian beam. A cross section of the beam seen at the dual-mode waveguide is shown in Fig. 52. It can be seen here that the beam profile is very nearly Gaussian. While a 79.15% power into the dual-mode waveguide aperture is a positive result it is decreased further when TE_{01} and TE_{03} modes, which do not propagate to the dual-mode waveguide, are accounted for. Considering the TE_{01} and TE_{03} modes which make up about 16% of the input beam in the real HSX transmission line system, the actual per cent power into the waveguide aperture decreases to 66.49%.

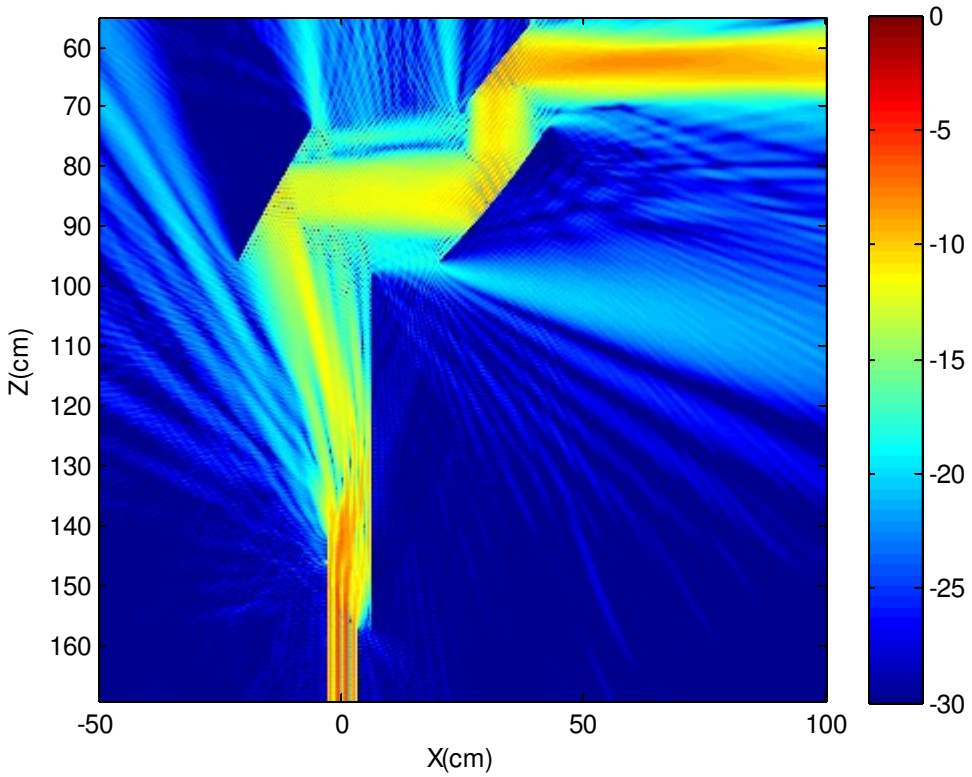

Fig 51. Side view of power density of TE_{02} mode beam propagated from the smooth-wall Vlasov launcher through the parabolic reflector, matching unit and polarizer of the HSX transmission system.

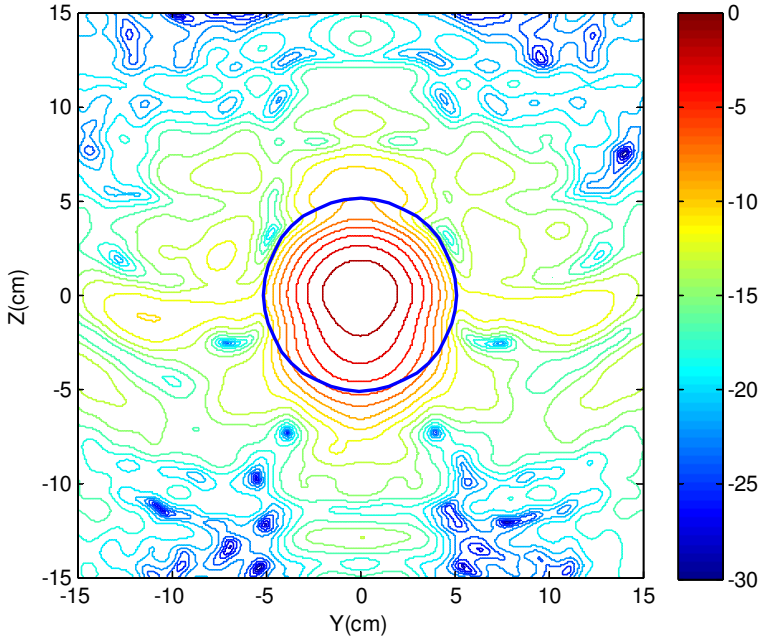

Fig. 52. Cross-section of power density of TE_{02} mode input to the smooth-wall launcher propagated to entrance of dual-mode waveguide in the HSX system.

On quick inspection the main opportunities for power loss appear to be due to the Vlasov launcher output not propagated in the main beam, spillover from the mirrors, and the beam itself not being focused sufficiently into the waveguide. Out of these three we expect the amount of the beam missing the waveguide and power lost in transmission from the Vlasov launcher to the parabolic mirror to be responsible for the majority of the power loss. While these should be the main factors, some additional spillover loss does occur.

The first step in understanding the power loss in the system was to find the power output from the Vlasov launcher that did not get directed into the parabolic mirror. To do this the fields on a cylinder that intersected the parabolic mirror at its parallel edges were simulated. It was found that approximately 94% of the power output from the Vlasov launcher is incident on the parabolic mirror. However, not all of the power will be converted to a Gaussian beam and transmitted to the dual-mode waveguide.

Moving through the system the total power in the beam was measured between mirrors M1 and M2 and found to be 90.97% of the total input power. From the output of the Vlasov launcher the beam was transformed into a roughly Gaussian beam after only the parabolic and ellipsoidal mirrors. While mirror M1 does increase the Gaussian content of the beam, it does not sufficiently narrow the beam to be input into the dual-mode waveguide.

Additionally because there is little observable beam divergence it can be approximated that a 5% power loss is due to spillover at mirror M1. Investigating the beam past M2, it was determined that there was a slight power loss such that only 86% of the power remained in the beam.

Investigating the power in the beam at the dual-mode waveguide revealed that the majority of power loss occurs between mirror M2 and the dual-mode waveguide. Only 79% of the TE_{02} power input to the HSX microwave transmission system is observed over the aperture of the dual-mode waveguide. Additionally, a power coupling coefficient of 0.9273 was calculated to the target Gaussian beam. Approximately 21% of the power in the beam that is reflected from M2 does not appear at the aperture of dual-mode waveguide. If a narrower beam was formed from mirror M2 more power could be directed into the waveguide, but the beam might not have the desired waist for optimum coupling. Additional losses also occur at mirror M2 and the polarizer due spillover.

E-3. HSX System with Perturbed-Wall Launcher

While the HSX transmission line system is designed for a smooth-wall Vlasov launcher, it is precisely this launcher which introduces inefficiency and losses into the system that could be removed with the use of a launcher with better output. However, since the HSX system was designed for the output beam from a smooth-wall launcher, any other output beam may not propagate well through the system. Several main issues exist in the output radiation patterns of smooth-wall Vlasov launchers. The output of the smooth-wall Vlasov launcher in the far-field is shown in Fig. 53.

First and probably most important is the main lobe. The output main lobe from the smooth-wall launcher is double-peaked and does not have the shape assumed by the ray-optics model. Only 77.5% of the power is in the main beam in the far-field. Additionally the azimuthal spread exceeds 180˚ and is therefore too large. The HSX system utilizes focusing and phase-correcting mirrors, but these introduce further loss into the system. Secondly, there are major diffraction losses and a large amount of the fields will be diffracted by the launcher cut and lost. Lastly the side lobes of the beam are substantial and result from the smooth-wall launcher radiation and from edge diffraction. It is very difficult to completely capture these large side lobes using most mirror systems and even when captured, they cannot be completely converted to a Gaussian beam with a simple mirror system. Perturbations can be applied to a smooth-wall Vlasov launcher to reduce these problems.

A perturbed-wall launcher was designed by Ungku Fazri Ungku Farid for possible use in the HSX system. The launcher has a length of 62.49 cm (corresponding to three and a half Brillouin zones) with a maximum perturbation size of 12.82% of the radius. The co-polarization of the far-field in the perturbed-wall launcher can be seen in Fig. 54. The differences in the radiation output of the launchers is described in Table IV. One main aspect of the perturbed-wall launcher is that it does not output as good a Gaussian beam with minimal side lobes as can be achieved with a longer perturbed-wall launcher. It should be noted that the polar exit angle changes slightly when perturbations are added to the launcher. This change in the polar exit angle was important and forced mirror M2 to be rotated slightly in order for the output beam to better propagate through the microwave transmission system. Overall the perturbations improved the percent of the power in the main lobe by 10% and improved the directivity by 3 dB. Additionally

the azimuthal angular spread is decreased to less than a third of the value of the smooth-wall launcher. There is an increase in the polar spread by approximately 7.4˚.

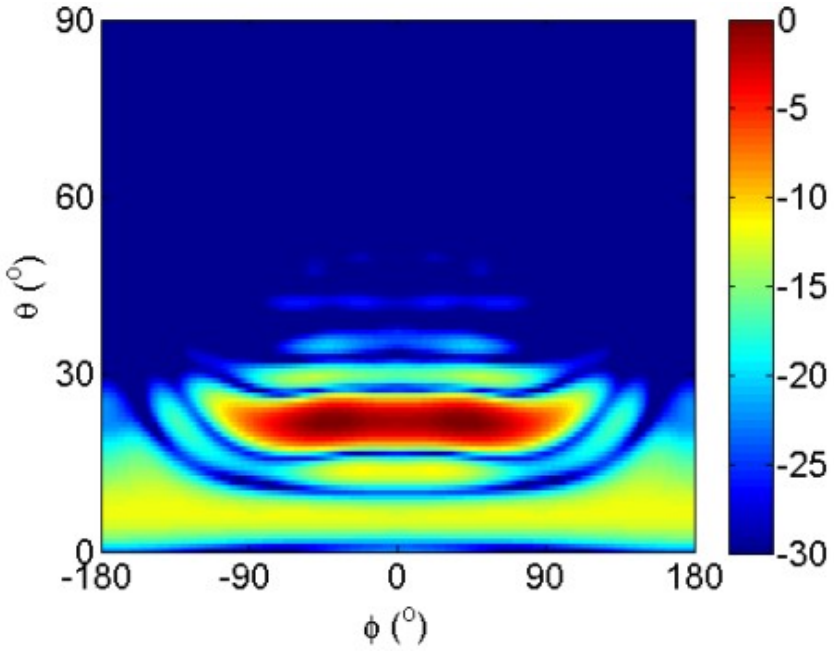

Fig. 53. The far-field pattern of $|E_\phi|$ co-polarization of the smooth-wall Vlasov launcher (in dB) obtained from Surf3d.

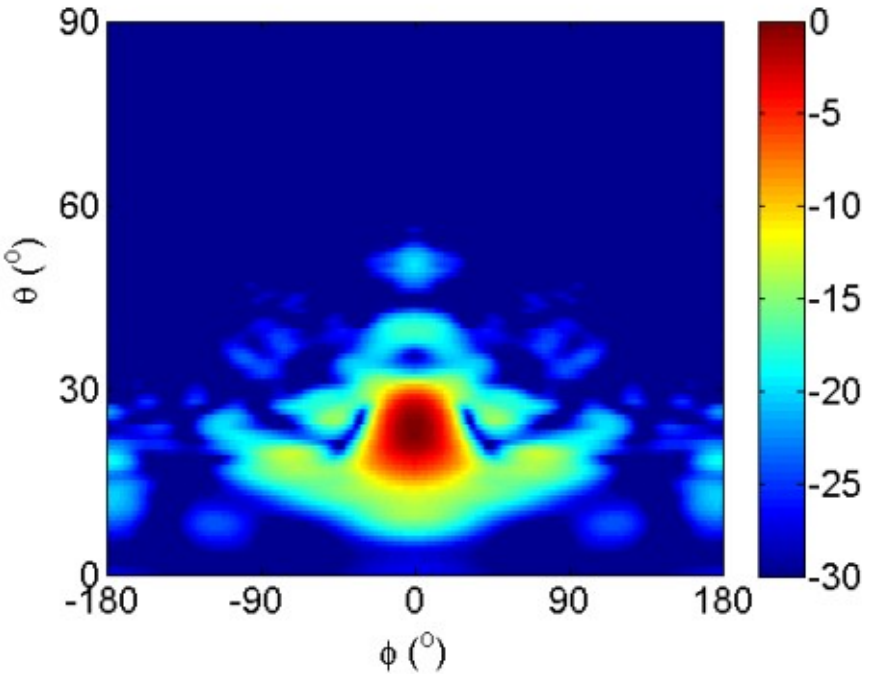

Fig. 54. The far-field pattern of $|E_\phi|$ co-polarization of the perturbed-wall HSX launcher (in dB) obtained from Surf3d.

Table IV. Summary of the Far Field Comparison of Launchers.

Launcher	Co-polarization (E_ϕ ¿					Cross-polarization (E_θ)	
	Polar Exit Angle	Power in Main Lobe	Directivity, D_ϕ	10 dB Angular Spread		$\|E_\theta\|_{max}$	Total Power
				Azimuthal, $\Delta\phi$	Polar, $\Delta\theta$		
Smooth-wall	23.1˚	77.53%	21.4 dBi	205.8˚	9.1˚	-21.4 dB	<0.01%
Perturbed-wall	24.0˚	87.61%	24.4 dBi	63.14˚	16.5˚	-20.6 dB	<0.01%

Although the output beam from the perturbed-wall launcher has improved characteristics, it will not work well with the current system without substantial changes. Change in the current system will entail significant expense and down time of the HSX stellarator. Using Surf3d, we were able to simulate a TE_{02} mode input into the perturbed-wall launcher and propagate the output beam through the HSX system. The results showed that indeed the power transmitted through the system was poorer for the new launcher than the old. However, a new design of the HSX transmission system using such a new launcher could be expected to have much higher

efficiency. Further, a new perturbed wall launcher could be designed specifically for an input into HSX.

E.4 Study of the Effect of an Increase in Baffle Length

At the end of summarizing our work, we include an additional interesting topic. Baffle length is normally calculated based on the geometrical optics model using Eq. (E.10) and here we obtain L_b = 15.63 cm for the HSX system. Using Surf3d we can vary the baffle length to see what will happen in simulation. We have found that the output power into the dual-mode waveguide increases slightly as L is increased to about 4.28 cm. It is somewhat surprising that the coupling efficiency C_p also increases as the baffle length increases and continues to increase as the length is increased to 7.5 cm. The coupled power is found from the product of the injected power and C_p which has a maximum increase of 3.6% at a baffle length increase if 4.28 cm. This is a modest but significant improvement for a simple design change.

Our simulation was based on incremental steps from L_B = 15.63 cm to a length 7.5 cm longer than this value. To better demonstrate the simulations, we have used two different Gaussian beam waists in calculating coupling efficiency, ω_0/a=0.59 and ω_0/a=0.64. Thus, there are two columns calculated coupling efficiency (C_p) versus baffle length change. We have also considered a baffle length one centimeter shorter than L_B. At the same time, the ratio of the output power to the input power is also calculated and recorded. The simulation results are shown in Table V.

Table V. Output Power and C_p Change with Baffle Length.

Baffle length compared with L_B (cm)	Output Power Ratio	Coupling Efficiency (0.59)	Coupling Efficiency (0.64)
-1.071	77.618%	0.9241	0.9362
-0.536	78.145%	0.9239	0.9362
0	78.591%	0.9273	0.9398
+0.536	79.006%	0.9277	0.9403
+1.071	79.304%	0.9315	0.9443
+1.606	79.548%	0.9322	0.9450
+2.142	79.734%	0.9329	0.9456
+2.677	79.854%	0.9369	0.9497
+3.213	79.937%	0.9376	0.9505
+3.748	80.048%	0.9379	0.9508
+4.034	80.058%	0.9383	0.9511
+4.284	80.254%	0.9419	0.9546
+4.819	80.007%	0.9421	0.9551
+5.3545	79.944%	0.9425	0.9555
+5.890	79.857%	0.9429	0.9559

+6.425	79.764%	0.9433	0.9564
+6.96	79.671%	0.9435	0.9566
+7.496	79.562%	0.9437	0.9568

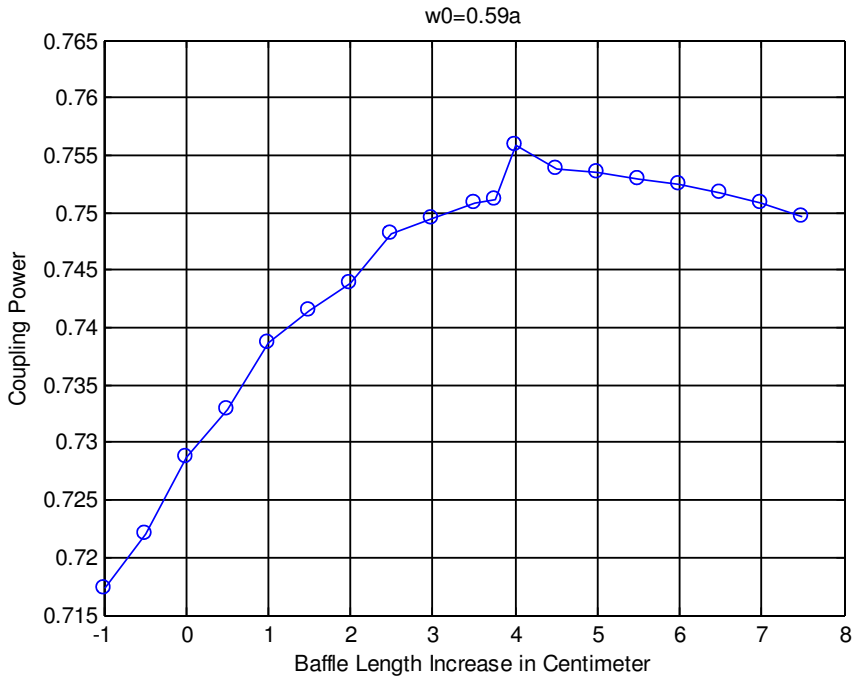

Fig. 55. Coupled power as a function of change in baffle length for $\omega_0/a = 0.59$.

F. Other Work.

Other work has been completed by the UW Group during this time period, but it will not be discussed in this report.

III. Brief Discussion Planned Future Work

The following topics will be pursued if graduate student help can be obtained.

A. Continued Work on Launchers and Mirror Systems for TE_{0n} Mode Gyrotrons

The work described in Sec. II-C will continue. In particular a perturbed-wall launcher will be developed for the TE_{02} mode at 28 GHz for possible use in HSX which would not require a new transmission system.

B. Continued work on a Traveling-Wave Resonator for increasing power for measurements on High power Components.

Work will continue on the simulation of the traveling wave resonator discussed in Sec. II-D. In particular the lateral shift of the reflected and diffracted beam will be studied by simulation. (Xiaodong Wang)

C. Microwave Resource to the US Magnetic Fusion Community

Even though the funding for this project has ended, we hope to continue to be a resource to the US gyrotron development and ECRH transmission line community for various problems which may arise in the area of our expertise.

IV. References

[1] Michael P. Perkins, Rong Cao, Jeffrey M. Neilson and Ronald J. Vernon; "A High Efficiency Launcher and Mirror System for Use in a 110 GHz $TE_{22,6}$ Mode Gyrotron," *Int. J. of Infrared and Millimeter Waves*, Vol. 28, No. 3, March 2007.

[2] Shaolin Liao and Ronald J. Vernon, "A Fast Algorithm for Wave Propagation from a Plane or a Cylindrical Surface," *Int. Journal of Infrared and Millimeter Waves*, Vol. 28, No. 6, pp. 479-490 (12), June 2007.

[3] Shaolin Liao and Ronald J. Vernon, "A Fast Algorithm for Computation of Electromagnetic Wave Propagation in Half-Space," IEEE Trans AP, Vol. 57, No. 7, pp. 2068-2075, 2009.

[4] Shaolin Liao, Ronald J. Vernon, and Jeffrey Neilson, "A High-Efficiency Four-Frequency Mode Converter Design with Small Output Angle Variation for a Step-Tunable Gyrotron," 33rd Int. Conf. on Infrared and Millimeter Waves, Pasadena CA, Sept. 2008.

[5] M. Thumm *et al.*, "A High-Efficiency Quasi-Optical Mode Converter for a 140-GHz 1-MW CW Gyrotron," *IEEE Trans. Elec. Dev.*, Vol. 52, No. 5, pp. 818–824, 2005.

[6] G. Denisov et al., “Development in Russia of High Power Gyrotrons for Fusion,” Nucl. Fus., Vol. 48, pp. 054007-1-5, 2008.

[7] A. Chirkov et al., “Multi-Frequency Gyrotron with High Efficiency Synthesized Waveguide Converter,” Tech Phys. Let., Vol. 33, pp. 350-352, 2007.

[8] A. Bogdashov, “High-efficient Mode Converter for “ITER” Gyrotron,” *Int. J. Infrared and Millimeter Waves*, Vol. 26, pp. 771-785, June 2005.

[9] G. G. Denisov *et al.*, “Concepts and Present Status for Multi-Mode Quasi-Optical Converters in Gyrotrons,” *Conference Digest, 2004 Joint* 29th *Int. Conf. on Infrared and Millimeter Waves and* 12th *Int. Conf. on Terahertz Electronics*, (Karlsruhe, Germany), pp. 483-484, Sept 2004.

[10] Jainbo Jin et al., "Novel Numerical Method for the Analysis and Synthesis of the Fields in Highly Oversized Waveguide Mode Converters", *IEEE Trans. Microwave Theory and Techniques*, Vol. 57, No. 7, pp. 661-1668, 2009.

[11] J. M. Neilson, “Optimal Synthesis of Quasi-Optical Launchers for High-Power Gyrotrons,” *IEEE Trans. Plasma Sci.*, Vol. 34, No. 3, pp. 635–641, 2006.

[12] J. Murphy, “Distortion of a Simple Gaussian Beam on Reflection from Off-Axis Ellipsoidal Mirrors,” *Int. J. Infrared and Millimeter Waves*, Vol. 8, No. 9, pp. 1165–1187, 1987.

[13] J. Neilson, “Surf3d and LOT: Computer Codes for Design and Analysis of High-Performance QO Launchers in Gyrotrons,” *Conference Digest, 2004 Joint* 29*th Int. Conf. on Infrared and Millimeter Waves and* 12*th Int. Conf. on Terahertz Electronics*, Karlsruhe, Germany, Sept. 2004.

[14] B. Katsenelenbaum and V. Seminov, “Synthesis of Phase Correctors Shaping a Specified Field,” *J. Radiotechnics and Electronics*, Vol. 12, pp. 223-231, 1967.

[15] B. Y. Rock and R. J. Vernon, “An Improved Design Methodology for Gyrotron Internal Mode Conversion System,” Oral presentation at the 33rd IRMMW-THz Conference in Houston, Oct., 2011.

[16] B.Y. Rock, Jeffrey M. Neilson, and Ronald J. Vernon, “A Power Optimizing Integrated Design of a Dual-Frequency Gyrotron Quasi-Optical Mode Converter,” *IEEE Transactions on Plasma Science*, V 40, No. 6, pp.1522-1529, June 2012.

[17] David S. Tax, Benjamin Y. Rock, Sudheer K. Jawala, Samuel C. Schaub, Michael A. Shapiro, Richard J. Temkin,, and Ronald J. Vernon, “Experimental Results for a Pulsed 110 GHz/124.5 GHz Megawatt Gyrotron,” *IEEE Transactions on Plasma Science*, V 42, No. 5, pp.1128-1134, May 2014.

[18] Jainbo Jin et al., "Novel Numerical Method for the Analysis and Synthesis of the Fields in Highly Oversized Waveguide Mode Converters," *IEEE Trans. Microwave Theory and Techniques*, Vol. 57, No. 7, pp. 661-1668, 2009.

[19] Jainbo Jin et al., "Theoretical Investigation of an Advanced Launcher for a 2 MW 170 GHz $TE_{34,19}$ Coaxial Cavity Gyrotron," IEEE Trans Microw. Theory & Tech. Vol. 54, No. 3, pp 1139-1145, 2006.

[20] G. G. Denisov et al., "Synthesized Quasi-Optical TE_{02}-HE11 Mode Converter," Conference Digest, 34th Int. Conf. on Infrared and Millimeter Waves and Terahertz Waves, Busan Korea, 2009.

[21] A.V. Chirkov et al., "Use of Huygens' Principle for Analysis and Synthesis for the Fields in Oversized Waveguides," *Radiophysics and Quantum Electronics*, Vol. 49, No. 5, pp. 344-353, 2004.

[22] Dimitry I. Sobolev and Gregory G. Denisov, "Principles of Synthesis of Multi-mode Waveguide Units", *IEEE Trans. Plasma Sci*., Vol. 38, No. 10, pp. 2825-2830, 2010.

[23] B. Y. Rock and R. J. Vernon, "An Improved Numerical Method for the Analysis of the Fields in a Deformed Waveguide," Joint 36th International Conference on Infrared, Millimeter, and Terahertz Waves, Houston, Oct. 2011.

[24] B. Y. Rock and R. J. Vernon, "A New Method for the Analysis of Perturbed Wall Waveguide Mode Converters," *IEEE Transactions on Plasma Science*, V 40, No. 6, pp.1502-1511, June 2012.

[25] Ungku Fazri Ungku Farid, B. Y. Rock, and Ronald J. Vernon, "A New Design of a Perturbed-Wall TE_{02} Launcher for a 60 GHz Gyrotron," Oral presentation at the Joint 33rd International Conference on Infrared, Millimeter, and Terahertz Waves, Houston, Oct. 2011.

[26] Ungku Fazri Ungku Farid, B. Y. Rock, and Ronald J. Vernon, "A Highly Oversized Perturbed-Wall TE_{02} Gyrotron External Launcher," Joint 37th International Conference on Infrared, Millimeter and Terahertz Waves, Wollongong, Australia, Sept. 2012.

[26] G.G. Denisov, A.V. Chirkov, V.I. Belousov, A.P. Gashtouri and G.I. Kalynova, "Synthesized Quasi-Optical TE_{02}-HE_{11} Mode Converter", *Conference Digest, 34th International Conference on Infrared, Millimeter and Terahertz Waves*, Busan, Korea, Sept. 2009.

[27] J. L. Milosevic and R. Vautey, "Traveling Wave Resonators," *IRE Transactions on Microwave Theory and Techniques*, pp. 136-143, April 1958.

[28] Benjamin Y. Rock and Ronald J. Vernon, "Deformation of Gaussian Beams by a Diffraction Grating," 33rd International Conf. on Infrared and Millimeter Waves, Busan, South Korea, Sept. 2009.

[29] Ungku Fazri Ungku Farid and Ronald J. Vernon, "Some Calculations Concerning Variable-Spacing Double-Disk Windows for Possible Use in Step-Tunable Gyrotrons," 32nd International Conference on Infrared and Millimeter Waves" Cardiff, United Kingdom, Digest pp. 890-891, Sept. 2-7, 2007.

[30] Bryan J. Fox, "Investigation of a Traveling-Wave Resonator for High-Power Component Testing for ITER," PhD Dissertation, University of Wisconsin at Madison, 2014.

[31] Kevin Felch, Comments on CPI Gyrotron Stability, Private Email Communication.

[32] Shuzhang Zhang and Theodor Tamir. "Spatial Modifications of Gaussian Beams Diffracted by Reflection Gratings", JOSA A 6.9 (1989), pp. 1368-1381.

[33] J. W. Radder, K.M. Liken, F.S.B. Anderson, and D.T. Anderson, “Hybrid transmission line for ECRH in the helically symmetric experiment,” *Int. J. Infrared Millim. Waves*, vol. 29, no. 4, pp. 360-372, Apr. 2008.

[34] Ungku Fazri Ungku Farid, "Theory and Algorithms for a Quasi-Optical Launcher Design Method for High-Frequency Gyrotrons," PhD Dissertation, University of Wisconsin at Madison, 2013.

V. Recent Publications Arising from this Work

David S. Tax, Benjamin Y. Rock, Sudheer K. Jawala, Samuel C. Schaub, Michael A. Shapiro, Richard J. Temkin,, and Ronald J. Vernon, "Experimental Results for a Pulsed 110 GHz/124.5 GHz Megawatt Gyrotron," *IEEE Transactions on Plasma Science*, V 42, No. 5, pp.1128-1134, May 2014.

Bryan J. Fox, B. Y. Rock, and Ronald J. Vernon, "Simulating a Traveling-Wave Resonator for High-Power ECRH Testing," Joint 38th International Conference on Infrared, Millimeter and Terahertz Waves, Mainz, Germany, Sept. 2013.

B. Y. Rock and R. J. Vernon, "A New Method for the Analysis of Perturbed Wall Waveguide Mode Converters," *IEEE Transactions on Plasma Science*, V 40, No. 6, pp.1502-1511, June 2012.

B.Y. Rock, Jeffrey M. Neilson and Ronald J. Vernon, "A Power Optimizing Integrated Design of a Dual-Frequency Gyrotron Quasi-Optical Mode Converter," *IEEE Transactions on Plasma Science*, V 40, No. 6, pp.1522-1529, June 2012.

U. F. Ungku Farid, B. Y. Rock and R. J. Vernon, "A Highly Oversized Perturbed-Wall TE_{02} Gyrotron External Launcher," Joint 37th International Conference on Infrared, Millimeter and Terahertz Waves, Wollongong, Australia, Sept. 2012.

Bryan J. Fox, B. Y. Rock and Ronald J. Vernon, "On Using a Traveling-Wave Resonator for High-Power Testing of Millimeter-Wave ECH Components," Joint 37th International Conference on Infrared, Millimeter and Terahertz Waves, Wollongong, Australia, Sept. 2012.

B. Y. Rock and R. J. Vernon, "An Improved Numerical Method for the Analysis of the Fields in a Deformed Waveguide," Joint 36th International Conference on Infrared, Millimeter, and Terahertz Waves, Houston TX, Oct. 2011

Ungku Fazri Ungku Farid, B. Y. Rock and R. J. Vernon, "A New Design of a Perturbed-Wall TE_{02} Launcher for a 60 GHz Gyrotron," Joint 36th International Conference on Infrared, Millimeter, and Terahertz Waves, Houston TX, Oct. 2011.

Shaolin Liao and Ronald J. Vernon, "A Fast Algorithm for Computation of Electromagnetic Wave Propagation in Half-Space," IEEE Trans AP. Vol. 57, No. 7, pp 2068-2075, 2009.

Michael P. Perkins and Ronald J. Vernon, "Two-Dimensional Phase Unwrapping to Help Characterize an Electromagnetic Beam for Quasi-Optical Mode Converter Design," Applied Optics, Vol. 47, No. 35, pp. 6606-6614, 2008.

M. P. Perkins and R. J. Vernon, "Mirror Design for Use in Gyrotron Quasi-Optical Launchers," *IEEE Transaction on Plasma Science*, Vol.35, No. 6, pp. 1747-1757, Dec. 2007.

Shaolin Liao and Ronald J. Vernon, "A Fast Algorithm for Wave Propagation from a Plane or a Cylindrical Surface," *Int. Journal of Infrared and Millimeter Waves*, Vol. 28, No. 6, pp. 479-490 (12), June 2007.

Michael P. Perkins, Rong Cao, Jeffrey M. Neilson and Ronald J. Vernon; "A High Efficiency Launcher and Mirror System for Use in a 110 GHz $TE_{22,6}$ Mode Gyrotron;" Int. J. of Infrared and Millimeter Waves; Vol. 28, No. 3, March 2007.

Shaolin Liao and Ronald J. Vernon, "Sub-THz Beam-Shaping Mirror System Designs for Quasi-optical Mode Converters in High-power Gyrotrons," *Journal of Electromagnetic Waves and Applications*, Vol. 21, No. 4, pp. 425-439 (15), 2007.

Qiuming Li and Ronald J. Vernon, "Theoretical and Experimental Investigation of Gaussian Beam Transmission and Reflection by a Dielectric Slab at 110 GHz," *IEEE Transactions on Antennas and Propagation*, Vol. 54, No. 11, pp 3449-3457, Nov. 2006.

VI. Publications in Preparation

"Design and Testing of a Mirror for Changing the Ellipticity of a Gaussian Beam," Bryan J. Fox and Ronald J. Vernon.

"Investigation of the Effect of Lengthening the Baffle for a Simple TE_{02}Vlasov Launcher," Xiaodong Wang and Ronald J. Vernon.

Appendix A. Biographical Sketch of Principal Investigator

Dr. Ronald J. Vernon, Professor Emeritus

Dr. Ronald J. Vernon, Professor Emeritus

Education: B.S. -1959, M.S. -1961, Ph.D. - 1965; all in Electrical Engineering from Northwestern University

Professional Positions: Assistant Prof. -June 1, 1965, Associate Prof.- July 1, 1969, Professor -July 1, 1978, Professor Emeritus -May, 2005; all in the Electrical and Computer Engineering Dept. of the University of Wisconsin – Madison, WI

Sept. 1, 1976 – June 30, 1977, summer 1975 and 1974: Research Engineer in the Engineering Research Division of Lawrence Livermore Laboratory, Livermore CA

Narrative:

Over the last thirty years Professor Vernon has been active in research directed toward high power microwave systems, primarily for electron cyclotron heating of fusion plasmas. His research group has designed the beam shaping reflector systems used inside two CPI gyrotrons

and a mirror optical unit used at General Atomics. The group has also developed new procedures for the design of such systems. They have developed reflector systems and mode converters for General Atomics and the UW HSX Stellarator. His group designed the beam shaping reflector system in the current depressed collector 1.25 MW gyrotron built at CPI, which is among the most efficient of such systems in the world.

Professor Vernon has taught both graduate and undergraduate courses primarily in the area of electromagnetic fields and waves, including antenna theory and microwave theory and techniques. He has taught both laboratory and lecture courses. His average student teaching evaluation rating for all his courses over the last twenty-five years is 4.8/5.0. He received the Polygon Award as Outstanding Teacher in the ECE Dept. in 1971 and the Holdridge Award for Teaching Excellence in May of 1998.

Professor Vernon is a US citizen born in Chicago, Illinois. He is a widower and has two adult children and two grandchildren.

After 39 years on the faculty of the UW Department of Electrical and Computer Engineering (30 years as full professor) he became an emeritus professor in May of 2005, but is still active in research, but no longer teaches.

Recent Publications Relevant to this Work:

David S. Tax, Benjamin Y. Rock, Sudheer K. Jawala, Samuel C. Schaub, Michael A. Shapiro, Richard J. Temkin,, and Ronald J. Vernon, "Experimental Results for a Pulsed 110 GHz/124.5 GHz Megawatt Gyrotron," *IEEE Transactions on Plasma Science*, V 42, No. 5, pp.1128-1134, May 2014.

Bryan J. Fox, B. Y. Rock, and Ronald J. Vernon, "Simulating a Traveling-Wave Resonator for High-Power ECRH Testing," Joint 38th International Conference on Infrared, Millimeter and Terahertz Waves, Mainz, Germany, Sept. 2013.

B. Y. Rock and R. J. Vernon, "A New Method for the Analysis of Perturbed Wall Waveguide Mode Converters," *IEEE Transactions on Plasma Science*, V 40, No. 6, pp.1502-1511, June 2012.

B.Y. Rock, Jeffrey M. Neilson, and Ronald J. Vernon, "A Power Optimizing Integrated Design of a Dual-Frequency Gyrotron Quasi-Optical Mode Converter," *IEEE Transactions on Plasma Science*, V 40, No. 6, pp.1522-1529, June 2012.

U. F. Ungku Farid, B. Y. Rock and R. J. Vernon, "A Highly Oversized Perturbed-Wall TE_{02} Gyrotron External Launcher," Joint 37th International Conference on Infrared, Millimeter and Terahertz Waves, Wollongong, Australia, Sept. 2012.

Bryan J. Fox, B. Y. Rock and Ronald J. Vernon, “On Using a Traveling-Wave Resonator for High-Power Testing of Millimeter-Wave ECH Components,” Joint 37th International Conference on Infrared, Millimeter and Terahertz Waves, Wollongong, Australia, Sept. 2012.

B. Y. Rock and R. J. Vernon, “An Improved Numerical Method for the Analysis of the Fields in a Deformed Waveguide,” Joint 36th International Conference on Infrared, Millimeter, and Terahertz Waves, Houston TX, Oct. 2011

Ungku Fazri Ungku Farid, B. Y. Rock and R. J. Vernon, “A New Design of a Perturbed-Wall TE_{02} Launcher for a 60 GHz Gyrotron,” Joint 36th International Conference on Infrared, Millimeter, and Terahertz Waves, Houston TX, Oct. 2011.

Shaolin Liao and Ronald J. Vernon, “A Fast Algorithm for Computation of Electromagnetic Wave Propagation in Half-Space,” IEEE Trans AP. Vol. 57, No. 7, pp 2068-2075, 2009.

Michael P. Perkins and Ronald J. Vernon, “Two-Dimensional Phase Unwrapping to Help Characterize an Electromagnetic Beam for Quasi-Optical Mode Converter Design,” Applied Optics, Vol. 47, No. 35, pp. 6606-6614, 2008.

M. P. Perkins and R. J. Vernon, “Mirror Design for Use in Gyrotron Quasi-Optical Launchers,” *IEEE Transaction on Plasma Science*, Vol.35, No. 6, pp. 1747-1757, Dec. 2007.

Shaolin Liao and Ronald J. Vernon, “A Fast Algorithm for Wave Propagation from a Plane or a Cylindrical Surface,” *Int. Journal of Infrared and Millimeter Waves*, Vol. 28, No. 6, pp. 479-490 (12), June 2007.

Michael P. Perkins, Rong Cao, Jeffrey M. Neilson and Ronald J. Vernon; "A High Efficiency Launcher and Mirror System for Use in a 110 GHz $TE_{22,6}$ Mode Gyrotron;" Int. J. of Infrared and Millimeter Waves; Vol. 28, No. 3, March 2007.

Shaolin Liao and Ronald J. Vernon, “Sub-THz Beam-Shaping Mirror System Designs for Quasi-optical Mode Converters in High-power Gyrotrons,” *Journal of Electromagnetic Waves and Applications*, Vol. 21, No. 4, pp. 425-439 (15), 2007.

Qiuming Li and Ronald J. Vernon, "Theoretical and Experimental Investigation of Gaussian Beam Transmission and Reflection by a Dielectric Slab at 110 GHz," IEEE Transactions on Antennas and Propagation, Vol. 54, No. 11, pp 3449-3457, Nov. 2006.

J. Shafii and R. J. Vernon, "Investigation of Mode Coupling Due to Ohmic Wall Losses in Overmoded Uniform and Varying-Radius Circular Waveguides by the Method of Cross Sections;" IEEE Transactions on Microwave Theory and Techniques, Vol. 50, pp 1361-1369, May 2002.

J. Shafii and R. J. Vernon, "Mode Coupling in Coaxial Waveguides with Varying-Radius Center and Outer Conductors," IEEE Trans. on Microwave Theory and Techniques, Vol. 43, No. 3, pp. 582-591, March 1995.

J. A. Lorbeck and R. J. Vernon, "A Shaped Reflector High-Power Converter for a Whispering-Gallery Mode Gyrotron Output," IEEE Trans. on Antennas and Propagation, Vol. 43, No. 12, pp. 1383-1388, Dec. 1995.

———

Benjamin Y. Rock and Ronald J. Vernon, "Deformation of Gaussian Beams by a Diffraction Grating," 33rd International Conf. on Infrared and Millimeter Waves, Busan, South Korea, Sept. 2009.

Shaolin Liao, Ronald J. Vernon, and Jeffrey Neilson, "A High-Efficiency Four-Frequency Mode Converter Design with Small Output Angle Variation for a Step-Tunable Gyrotron," 33rd International Conf. on Infrared and Millimeter Waves, Pasadena CA Sept. 2008.

Shaolin Liao, Ronald J. Vernon, and Jeffrey Neilson, "A Four-Frequency Mode Converter with Small Output Angle Variation for a Step-Tunable Gyrotron," EC-15 Conf., Yosemite, CA**.,** March 9-13, 2008.

Ungku Fazri Ungku Farid and Ronald J. Vernon, "Some Calculations Concerning Variable-Spacing Double-Disk Windows for Possible Use in Step-Tunable Gyrotrons," 32nd International Conference on Infrared and Millimeter Waves" Cardiff, United Kingdom, Sept. 2-7, 2007, Digest pp. 890-891.

S. L. Liao and R. J. Vernon, "The Near-Field and Far-Field Properties of the Cylindrical Modal Expansions with Application to the Image Theorem," *Joint 31st Infrared and Millimeter Waves and 14th International Conference on Terahertz Electronics*, Shanghai, China, IEEE MTT, Sep. 18-22, 2006.

S. L. Liao and R. J. Vernon, "The Cylindrical Taylor-Interpolation FFT Algorithm," *Joint 31st Infrared and Millimeter Waves and 14th International Conference on Terahertz Electronics*, Shanghai, China, IEEE MTT, Sep.18-22, 2006.

M.P. Perkins and R.J. Vernon, "Iterative Design of a Cylinder-Based Beam-Shaping Mirror Pair for Use in a Gyrotron Internal Quasi-Optical Mode Converter," 29th Int. Conf. on Infrared and Millimeter Waves, Karlsruhe, Germany, Digest pp. 489-490, Sept. 2004 .

R. Cao, M.P. Perkins, R.J. Vernon, and J.M. Neilson, "Design of a High Efficiency Launcher and Mirror System for Use in a 110 GHz $TE_{22,6}$ Mode Gyrotron" R. Cao, M.P. Perkins, R.J. Vernon, and J.M. Neilson; 29th Int. Conf. on Infrared and Millimeter Waves, Karlsruhe, Germany, Digest pp. 487-488, Sept. 2004.

Synergistic Activities

Professor Vernon has attended and made presentations at many international gyrotron workshops and US gyrotron community meetings (approximately 1-2 per year) over the last 25 years.